Regulation of Effector and Exhausted $CD8^+$ T Cell Fates

Pei Hsuan Wu

A thesis

submitted in partial fulfillment of the

requirements for the degree of

Master of Science

University of Washington

2025

Committee:

Hao Yuan Kueh

Thelma Escobar

Program Authorized to Offer Degree:

Bioengineering

University of Washington

Abstract

Regulation of Effector and Exhausted CD8$^+$ T Cell Fates

Pei Hsuan Wu

Chair of the Supervisory Committee:

Hao Yuan Kueh

Department of Bioengineering

The adaptive immune system protects the body against a wide range of threats by mounting specific immune responses tailored towards pathogens. Cytotoxic CD8$^+$ T cells, a population within the adaptive immune system, play a crucial role in clearing infections by eliminating infected or malignant cells. Depending on the infectious contexts and external stimuli, CD8$^+$ T cells differentiate into different functional states. Upon antigen encounter, during an acute infection, CD8$^+$ T cells differentiate into short-lived effector states with cytolytic activity as well as long-lasting memory cells that persist after infection clearance and can mount rapid and strong responses upon re-challenge. In a chronic context, persistent antigen stimulation drives CD8$^+$ T cells into an exhausted state, characterized by reduced effector function, loss of self-renewal and dysfunctional properties. T cell exhaustions are often linked with poor clinical prognosis and

impaired pathogen clearance. In this thesis, I will focus on understanding how differences in antigen affinity and dosage affect $CD8^+$ T cell effector differentiation decisions and understand the epigenetic mechanisms underlying their terminal differentiation and exhaustion fate commitment. In Chapter 1, I will briefly introduce the immune system and $CD8^+$ T cells. In Chapter 2, I will focus on how $CD8^+$ T cells perceive the affinity of pMHC to regulate their effector gene expression. And finally, in Chapter 3, I will discuss the epigenetic molecular mechanisms involved in fate commitment.

ACKNOWLEDGEMENTS

I would first like to express my deepest gratitude to my mentors and advisor. I have been incredibly fortunate to be surrounded by such caring, supportive, and inspiring individuals. To my industry mentors, Olga Sharapova and Cecilia Go, thank you both for inspiring me to pursue a further degree and supporting my development as a scientist. To my committee member, Thelma Escobar, thank you for your thoughtful discussions and valuable feedback on the CUT&RUN data.

To my advisor, Kueh, thank you for being such a thoughtful and understanding mentor. Your genuine care for the growth of your mentees, your willingness to support me through uncertain times, and your countless hours of guidance have been invaluable. I'm especially grateful for the creative freedom you gave me to pursue questions that truly intrigued me, and for your insights when encountering challenging research problems. I am immensely thankful to have you as my advisor.

I would also like to thank Matthew Wither, Elisa Maynor, and Kathleen Abadie for being such wonderful mentors. Thank you for helping me get started in the lab, troubleshooting experiments with me, and engaging in insightful discussions that advanced my thinking.

To everyone in the Kueh Lab, Arjun Kumar, Morgan Bean, Katie Denecke, Madeline Wong, Will White, Nancy Gao, Paul Leanza, and Lihua Chen, thank you all for your advice, collaboration and support, and for making the lab such an enjoyable space to be in. A special thank you to Arjun Kumar, for helping me get set up in the lab and for the mentorship you have provided. To Morgan Jones and Nelli Aydinyan from the Escobar Lab, thank you for being fantastic collaborators and for the many brainstorming sessions, especially when our code refused to cooperate.

I also want to acknowledge the animals whose lives contributed to this research and to thank the husbandry staff in the UW animal facilities for their dedicated care.

Lastly, to my friends and family: thank you all for your unwavering support, encouragement, and companionship throughout this journey. I could not have done this without you, and I am truly grateful.

Chapter 1. Introduction

1.1 Overview of our immune system and CD8$^+$ T cells

Our immune system is a remarkable defense network that protects the host against foreign pathogens and cancer. It comprises two parts: innate and adaptive immunity. The innate immunity serves as the body's first line of defense and is nonspecific to any pathogens. It recognizes and responds to molecular patterns shared by many microbes but absent in the host[1], allowing a quick response. The second line of defense is the adaptive immunity, which exhibits a high level of specificity towards antigens, a unique feature found on the surface of pathogens. Once it detects the presence of antigens, the adaptive immune system mounts a specific response to eliminate pathogens[1]. The adaptive immune system also possesses a remarkable memory property, allowing it to remember antigens from past infections and respond more quickly and strongly upon future re-exposure.

Cytotoxic T cells, or CD8$^+$ T cells, are a central part of our adaptive immune system, acting as powerful effector cells in anticancer and infection responses. Naive CD8$^+$ T cells express a unique cell surface receptor, the T cell receptor (TCR), each of which recognizes specific peptides presented by class I of the major histocompatibility complex (MHC)-derived molecules on antigen-presenting cells (APC)[2,3]. These naive CD8$^+$ T cells continuously circulate throughout the bloodstream and lymphoid organs, making contact with the APC and surveilling our body for threats[4]. In the absence of infection, the peptides-MHC (pMHC) presented on APC are self-derived endogenous peptides, which do not activate naive CD8$^+$ T cells. On the other hand, during an infection, APCs can digest and process pathogens, presenting foreign antigen peptides on their

MHCs. These foreign pMHC can be recognized by antigen specific $CD8^+$ T cells, and along with other co-stimulatory signals, the naïve $CD8^+$ T cells activate, proliferate and differentiate into effector cells capable of killing.

The strength of TCR to pMHC determines whether $CD8^+$ T cells become activated, serving as a key mechanism to prevent inappropriate responses against healthy tissues. While the binding strength of TCR to self pMHC is typically weak, its affinity for foreign antigens pMHC is on average 10 times higher, with a slower dissociation rate[5]. As TCR engagement triggers a series of downstream events, the slower dissociation rate allows late downstream signaling events to happen[6,7], overcoming the temporal lag between ligand binding and TCR signaling[8,9]. This mechanism, known as kinetic proofreading, allows $CD8^+$ T cells to discriminate between foreign and self and to activate only in the presence of infections[8–11].

The activation of $CD8^+$ T cells require three signals, including i) TCR - pMHC signals ii) co-stimulatory signals from the APC[12,13], and iii) inflammatory cytokines such as IL-12 or IFNα/β[14]. Once naive T cells receive those signals, they activate and proliferate, differentiating into different subsets. In an acute infection, the majority differentiate into effector cells that migrate throughout the body to clear off the infections[2,3,15]. Effector $CD8^+$ T cells use their TCR to identify infected cells that are expressing antigen-derived pMHCs. Once identified, they kill the infected cells by secreting granules containing granzymes and perforin; the perforin induces pores in the target cells' membranes and allows granzymes to enter and trigger cell apoptosis[2,3]. Following clearance of infection, many of the effector cells die; however, a portion differentiates into memory cells[15,16]. Memory cells remember past infections and rapidly respond upon re-exposure to the same antigen

by proliferating quickly, providing future protection. However, in the context of persistent threats such as chronic infections or cancers, $CD8^+$ T cells experience ongoing antigen stimulation, which prevents them from differentiating into memory cells but drives differentiation into exhausted T cells[17,18]. Exhausted T cells exhibit a distinct transcriptional and epigenetic profile from effector and memory cells, with progressive loss of their effector and self-renewal functions [19]. As $CD8^+$ T cells progress to exhaustion with prolonged antigen exposure, they upregulate their expression of inhibitory receptors, such as Tim3, CTLA4, and LAG3. These inhibitory receptors, when engaged, dampen their functions to prevent tissue damage from an overactive immune response.[17,18] Exhaustion prevents effective control of infection and tumors and contributes to the failure to clear cancers and chronic infections.

$CD8^+$ T cells' high selectivity towards threats versus self and their ability to confer lifelong immunity have made them a significant focus in many immunotherapies, autoimmune and anticancer research. Current research continues to explore how $CD8^+$ T cells sense and integrate external signals, activate distinct gene programs and differentiate into various functional subsets. Through a better understanding of how $CD8^+$ T cells function, we can inform better vaccine designs and T cell-based immunotherapies in combating autoimmune, cancers and chronic diseases.

Chapter 2:

pMHC affinity regulates T cell effector programming kinetics through NFAT and Erk signaling pathways

2.1 Abstract

Our immune system serves as the body's first line of defense against infections and other pathogens. Naive $CD8^+$ T cells recognize foreign peptides presented on antigen-presenting cells through their T-cell receptor (TCR), rapidly activating and proliferating to eliminate foreign threats upon an infection. While varying peptide-major histocompatibility complex (pMHC) affinities are known to drive distinct differentiation, how pMHC affinity is sensed and translated into effector programming is unknown. As NFAT and Erk signaling pathways act downstream of TCR, with their later (9hrs post-stimulation) dynamics conveying pMHC information, we investigated their role in translating pMHC affinity in effector programming. We found that pMHC affinity is reflected in the temporal regulation of effector genes, CD25 and IRF4. High-affinity pMHC induced faster, stronger and more sustained CD25 and IRF4 expression; in contrast, low-affinity pMHC resulted in delayed, lower CD25 and IRF4 expression and failed to maintain them. Furthermore, we found that pMHC affinity relied on NFAT and Erk levels to regulate the activation rate of effector genes but not their maintenance. These findings revealed a key role of NFAT and Erk signaling pathways in decoding pMHC affinity, leading to distinct temporal expression of effector programming and potentially offering insights into how pMHC affinity may bias T cell differentiation fates.

2.2 Introduction

During an acute infection, $CD8^+$ T cells are activated and can differentiate into effector and memory T cells. The strength of TCR's interaction with pMHC directly influences $CD8^+$ T cell activation and fate decision [20–22]. The asymmetric division model suggests that strong TCR-pMHC interactions favor T cell activation, expansion and differentiation into short-lived effector cells. In contrast, weaker interactions lead to lower expansion and lesser differentiation into effector cells[23]. Similarly, the TCR strength signal model proposes that the generation of effector and memory cells depends on the overall strength of antigen, co-stimulation and pro-inflammatory cytokines signals[20]. Other studies have also demonstrated that lower-affinity pMHC is sufficient to activate T cells and enhance $CD8^+$memory development[24–26]. Together, these findings suggest a tight coordination between the strength of ligand-TCR interactions and $CD8^+$ T cells expansion and differentiation. However, the mechanism by which $CD8^+$ T cells sense ligand affinity to drive distinct differentiation and functional responses remains unclear.

TCR engagement with pMHC activates a cascade of signaling pathways downstream within minutes, including nuclear factor of activated T cells (NFAT) and extracellular signal-regulated kinase (Erk) pathways[27]. The NFAT, a transcriptional factor (TF), when activated, can translocate into the nucleus from the cytoplasm and activate downstream genes. At the same time, Erk can phosphorylate and activate TF AP-1, leading to downstream gene expression[27]. Using fluorescence-tagged NFAT and Erk, along with fluorescence microscopy, Withers et al. demonstrated that the late dynamics of Erk and NFAT levels, defined as 9 hrs post-stimulation, can convey pMHC information leading to distinct transcriptional programs[28].

In this study, we investigated how pMHC affinity influences the $CD8^+$ T cell effector program. We looked at CD25 and IRF4 as part of the effector program, as CD25 is initially upregulated following TCR stimulation, the sustained expression of CD25 biases $CD8^+$ T cells into a more terminal effector state[29]. At the same time, IRF4 correlates with the strength of TCR signals and promotes the formation of effector T cells[30]. Additionally, we asked whether NFAT and Erk play a role in translating the effects of pMHC affinity during the early effector programming phase. We found that while both high and low affinity pMHC were able to elicit CD25 and IRF4 expression, they differ in their kinetics. Cells stimulated with high affinity pMHC express CD25 and IRF4 faster, stronger and longer. The expression of CD25 and IRF4 is further prevented when NFAT and Erk are inhibited early at the time of stimulation. However, later inhibition of NFAT and Erk did not impact CD25 and IRF4 expression. These results suggest that pMHC affinity regulates effector gene activation kinetics through early NFAT and Erk signaling pathways.

2.3 Results

2.3.1 Temporal control of activation decodes pMHC affinity

Utilizing $CD8^+$ T cells isolated from the P14 mice, which express transgenic TCRs specific for lymphocytic choriomeningitis virus (LCMV) peptides, we stimulated them with peptides of varying affinity (Agonist: M9C, K_D = 2.3uM; Partial agonist: L6F, K_D = 19uM). This assay allowed us to investigate how differences in pMHC affinity affect the effector gene program. Additionally, we stimulated cells with varying dosages of the agonist (20, 2, 0.2 pmol) and partial agonist (20 pmol) to see if pMHC dosages also play a role in influencing the effector gene program. We stained for CD25 and IRF4 and measured their expression with flow cytometry at 4, 8, 16 and 30 hours post-stimulation. While both agonist and partial agonist elicited CD25 and IRF4

expression, their activation profile and magnitude differed with different pMHC affinity but not dosage. **(Fig 2.1B)**. Cells stimulated with an agonist exhibited a larger proportion of $CD25^+$ and $IRF4^+$ cells with a faster activation rate compared to those stimulated with the partial agonist. Agonist stimulated cells reached maximum CD25 and IRF4 expression 10 hrs post stimulation, while those stimulated with partial agonist reached maximum expression at 16 hrs, highlighting the more rapid activation induced by the agonist (**Fig 2.1 C, D).** The cells stimulated with agonist also sustained CD25 and IRF4 expression throughout the time course, while the partial agonist failed to maintain their CD25 expression **(Fig 2.1C)**. Our findings showed that affinity, but not the dosage of pMHC, can influence T cell activation, consistent with the kinetic proofreading model of TCR signaling. However, while both affinities were capable of activating cells and elicited the same effector gene program, the affinity strengths impact the temporal activation and persistence of these effector genes. This shared yet temporally distinct regulation of effector genes may enable a broader immune response while contributing to the divergence of fates, as previously suggested by scRNA-seq data[31]. The high and sustained levels of IRF4 seen with agonist stimulation may explain why high-affinity pMHC does not promote memory cell differentiation, as elevated levels of IRF4 limit the development of memory-like T cells[30,32].

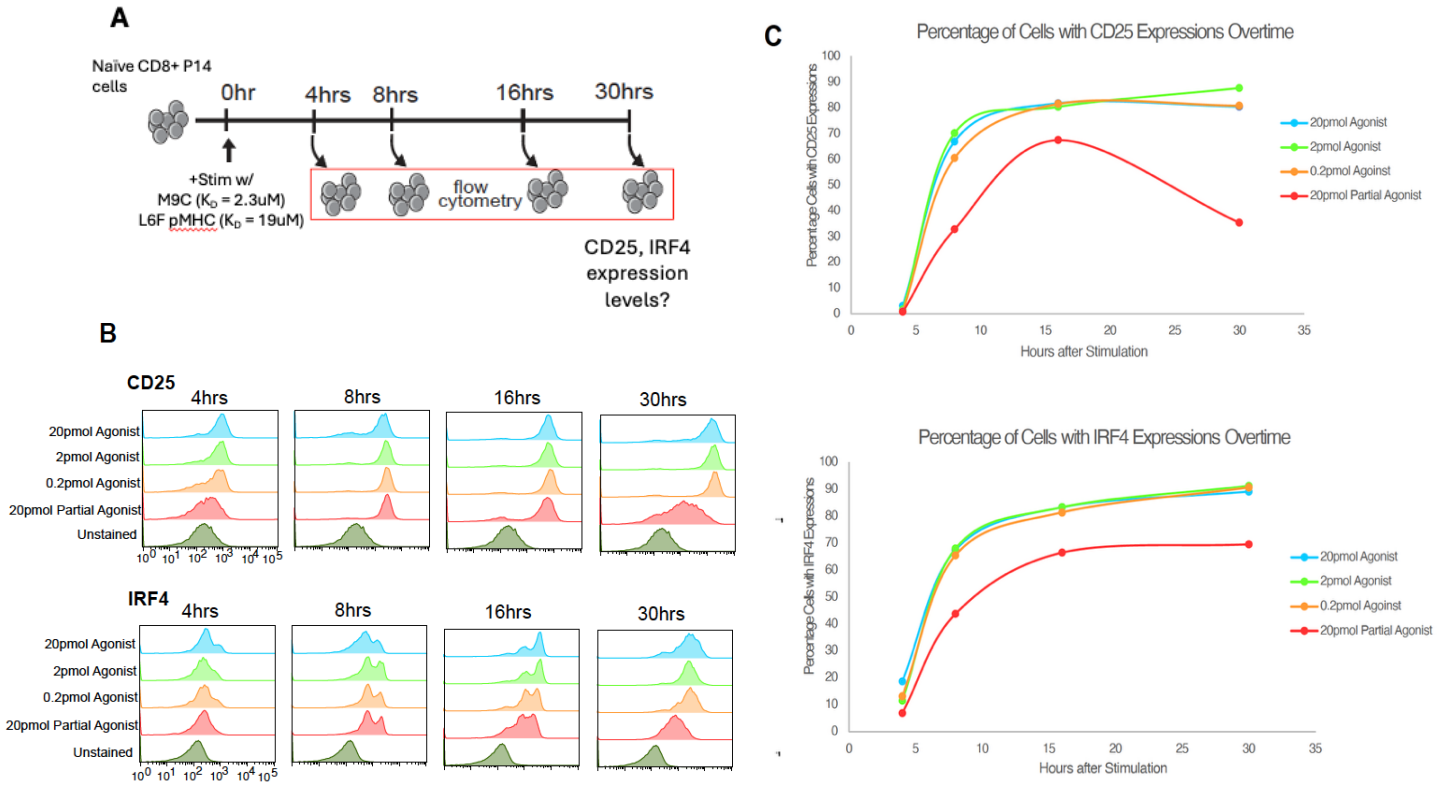

Figure 2.1. ***Cells stimulated with high-affinity pMHC activated effector genes CD25 and IRF4 faster, stronger and longer than low-affinity pMHC.*** (A) Experimental workflow. (B) Flow cytometry plot of CD25 (top) and IRF4 (bottom) at indicated time points for cells stimulated with high-affinity agonist pMHC (20, 2, 0.2pmol) and low-affinity partial agonist (20pmol). (C) The percentage of cells with CD25 or IRF4 expression was plotted against stimulation time. Expression of CD25 and IRF4 is independent of pMHC dosage but dependent on pMHC affinity. The agonist elicited faster, stronger and longer CD25 and IRF4 expression than the partial agonist.

2.3.2 Early NFAT and Erk regulate the dynamics of effector programs

Early differences (0 – 8hrs) in the kinetics of CD25 and IRF4 expression were influenced by pMHC affinity. Furthermore, their expression was maintained only with agonist but failed to be maintained with partial agonist stimulation. Given that NFAT and Erk late dynamics (9+hrs post stimulation) decode pMHC information[28], we asked whether they play a role in the differences in the initiation and maintenance of CD25 and IRF4 expression mediated by the pMHC affinity. We

stimulated cells with various doses and affinities of pMHC and inhibited with NFAT inhibitor (CsA) and/or Erk inhibitor (MEKi) at an early point (0hrs) and stained for CD25 and IRF4 expression at 16 hrs; or inhibited at a later time point (9hrs) and stained at 30 hrs.

Both cells stimulated with agonist and partial agonist showed a reduction in their CD25 and IRF4 expression with NFAT inhibitor and, to a smaller extent, with Erk inhibitor when inhibited at 0 hr **(Fig 2.2B)**, showing that the activation of CD25 and IRF4 depended on both early NFAT and Erk levels. On the other hand, CD25 and IRF4 expression did not decrease with late inhibition, especially for cells stimulated with an agonist; instead, their expression was either maintained or increased **(Fig 2.2C)**. These results suggest that the maintenance of CD25 and IRF4 is independent of NFAT and Erk signaling but may depend on another factor that could sense affinity. Interestingly, cells stimulated with agonists and treated with Erk inhibitors at a late timepoint had higher expression of CD25 and IRF4 than cells not treated with inhibitors. It is plausible that this other factor can cooperate with and bind to AP-1, a transcription factor downstream of Erk signaling, to activate genes. Therefore, late inhibition of Erk resulted in the absence of AP-1, allowing this factor to become more available to bind to the regulatory regions of CD25 and IRF4 and enhance their expression. While late inhibition did not affect CD25 and IRF4 expression for cells stimulated with agonists, cells stimulated by partial agonists showed a reduction in CD25 and IRF4 expression; however, not to the same extent as early inhibition **(Fig 2.2C)**. This could be due to partial agonists failing to amplify the other factor maintaining CD25 and IRF4 expression, such that their expression may still be dependent on later NFAT and Erk signaling pathways. Another hypothesis may be that, as partial agonists activate cells more slowly, so do the NFAT and Erk signaling, making CD25 and IRF4 expression still dependent on NFAT and Erk in later timepoints.

Overall, these data point to the role of NFAT and Erk signaling in modulating the timing of effector gene activations in response to pMHC affinities but not the maintenance.

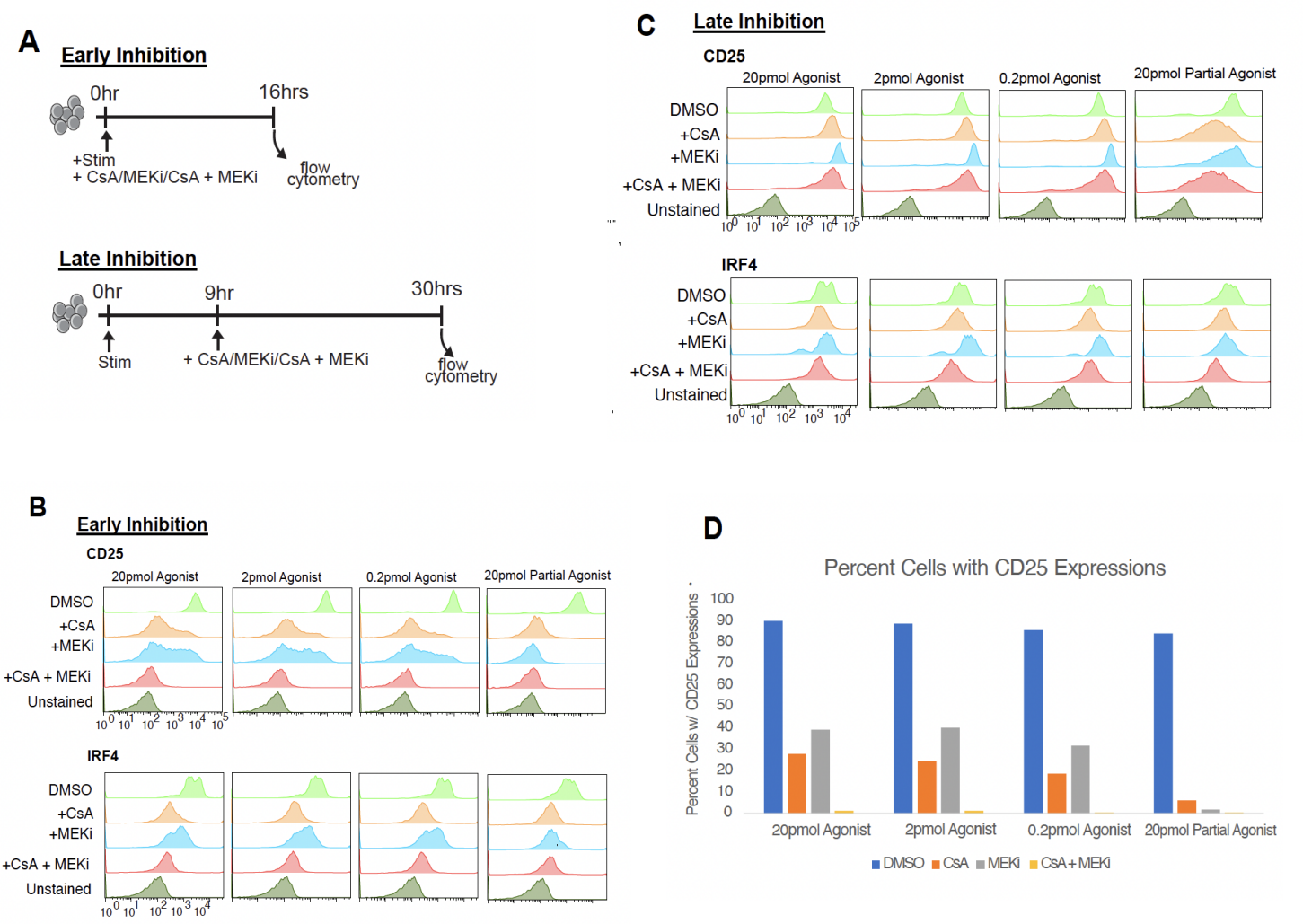

Figure 2.2. ***Early NFAT and Erk inhibition significantly reduced the expression of CD25 and IRF4.*** (A) Experimental overview. Cells were stimulated with 20, 2, 0.2 pmol agonist or 20pmol partial agonist at 0hr. The NFAT inhibitor (CsA), Erk inhibitor (MEKi) or both were added either at 0 hr (early inhibition) or 9 hrs post-stimulation (late inhibition), and CD25 and IRF4 expression were analyzed by flow cytometry at 16hrs for early inhibited cells or 30 hrs for late inhibited cells. (B) Flow cytometry plots of CD25 (top) and IRF4 (bottom) for early inhibited cells. (C) Flow cytometry plot of CD25 (top) and IRF4 (bottom) for late inhibited cells. (D) Percentages of cells with CD25 expression plotted against pMHC affinity, dose with different inhibitor conditions.

2.4 Discussion

The influence of peptide–MHC (pMHC) affinity on T cell activation and differentiation has been extensively studied. High-affinity peptides are traditionally thought to overcome the kinetic proofreading constraints of TCR, thereby promoting T cell activation. However, recent evidence shows that even low affinity pMHCs can activate T cells, but bias towards memory differentiation. Regardless of stimulation strength, the activated cells exhibit cytolytic activity and engage in the same transcriptional pathways, albeit to different degrees[31]. These observations raised the question of how differences in pMHC affinity are sensed and translated downstream to modulate effector gene expression and ultimately influence distinct T cell fates.

Here, we demonstrated that peptide affinity regulates the kinetics of effector genes, thereby tuning their expression levels, timing, and duration. While high and low affinity peptides can activate T cells, they differ in their activation dynamics. We found that high affinity pMHC elicited faster, stronger and longer expression. In contrast, low affinity pMHC failed to induce the same levels of gene expression and maintain them. Through NFAT and Erk inhibition, we further demonstrated that peptide affinity is conveyed through early NFAT and Erk signaling pathways downstream of TCR, influencing the temporal activation of CD25 and IRF4.

While we only looked at the expression of two genes, CD25 and IRF4, the results suggest broader implications for how pMHC affinity regulates effector gene expression and influences cell fates through early NFAT and Erk signaling. Competing transcription factors (TFs) are known to shape $CD8^+$ T cell differentiation and memory potential[20]. During an infection, elevated expression of some TFs, such as Tbet and BLIMP-1, biases cells toward effector phenotypes[32]. Given that IRF4

promotes the expression of T-bet and BLIMP-1[33], it is plausible that high-affinity pMHC not only upregulates but also sustains the expression of these and other effector-associated TFs, thereby driving cells towards effector differentiation. Additionally, how pMHC affinity modulates the expression levels of memory-related TFs remains an interesting question to explore in the future.

As the experiment was not long enough for cells to differentiate, additional longer-term experiments would need to be performed to validate the relationship between affinity, early gene expression, and cell fates. Furthermore, as pMHC affinity is conveyed downstream through early NFAT and Erk signaling, it would be interesting to see how early inhibition of NFAT and Erk would impact T cell differentiation decisions and whether we can selectively skew memory T cell differentiation.

2.5 Methods

Mice

Dual-Pathway Reporter (DPR) B6 mouse strain ($Rosa26^{LSL\text{-}DPR/LSL\text{-}DPR}$) was generated by Biocytogen Corp. using Rosa26 targeting vectors with reporter cassette encoding Erk-KTR fused with mTagBFP2, H2B fused to near-infrared fluorescent protein (iRFP), and residues 1 to 399 of mouse NFATc2 fused with mRuby3. Rosa26LSL-DPR/LSL-DPR mice were crossed with LCMV-specific transgenic TCR (P14) mice and Cre-ERT2 mice to generate Rosa26LSL-DPR/Cre-ERT2 mice with P14 TCR specificity. Eight-week-old male and female mice were injected with four doses of tamoxifen over four consecutive days and used for imaging experiments 4 - 12 weeks later. $Rosa26^{LSL\text{-}DPR/LSL\text{-}DPR}$ with P14 TCR mice was used for nonimaging experiments.

pMHC - Coated Plates

Plates were coated with 2 ug RetroNectin (TaKaRa Cat.no. T110A) and 1 ug anti-LFA1, and 2ug NeutrAvidin (Thermo Fisher Scientific, Cat # 31000) overnight at 4C. Plates were washed with PBS (3x100uL) and blocked with 1% BSA in PBS at 37 C for 1 hr the following day. pMHC corresponded to 20pmol, 2pmol and 0.2pmol of biotinylated monomeric H-2D^{b} MHC with KAVYNFATM (M9C) - agonist, or 20pmol and 0.2pmol monomeric H-2D^{b} MHC loaded with KAVYNLATC (L6F) - partial agonist, were prepared and added to each well and incubated at 4C for 1.5hrs.

CD8^{+} T cell Isolations

Spleens were harvested and single cell suspension of splencytes was generated by manual dissociation between rough microscope slides and filtered over 40 um cell strainers. Red blood cells were lysed for 5 minutes at room temperature using RBC lysis buffer (1mM EDTA, 10mM NaHCO3, 150mM NH4Cl) and quenched with HBH buffer (HBSS + 0.5% BSA). Cells were resuspended in Fc blocking buffer (2.4G2 supernatant in HBH) and incubated on ice for 15 min. CD8^{+} T cells were isolated using Miltenyi CD8^{+}negative selection kit (Miltenyi #130-104-075).

***In Vitro* T cells assay**

The seeded pMHC-coated plate was washed 2x with PBS and 80k purified CD8^{+}cells were seeded per well. The plate was spinned at 50g for 1min and incubated at 37C, 5% CO2. Cells were cultured in AIM-V media (Thermo Fisher Scientific, Cat # 12055091) with 50uM BME,.

MEKi and CsA Perturbation

Cells were treated with 2uM, 0.6uM, 0.2uM and 0.07uM CsA (Sellekchem Cat no 52286) or MEKi (Trametinib. Sellekchem Cat no S2673) or DMSO (0.1%) at 0hrs or 9hrs.

Flow Cytometry

Cells were incubated in Fc blocking solution (2.4G2 supernatant in HBH) for 15 min on ice, then stained with extracellular antibodies containing 0.5 µl anti-CD25 or 1 µl anti-CD279 (PD-1) per sample for 20 min at 4 °C in the dark. Cells were permeabilized and stained with 0.5 uL anti-IFR4 per well. Briefly, cells were washed with Perm/wash buffer and incubated 10 min at room temperature. Cells were washed 1x with HBH and stained with anti-IRF4 for 20min at RT. Cells were analyzed on an Attune Nxt cytometer (Thermo Fisher Scientific).

Chapter 3:

PRC1 and PRC2 cooperate to lock down terminal T cell exhaustion by heritably maintaining repressive chromatin modifications at memory gene loci

*This chapter is adapted from the manuscript in collaboration with the Escobar lab: **Polycomb Repressive Complexes jointly enforce Tcf7 silencing and commitment to a terminally exhausted T cell fate**

Elisa C. Clark[1,7], Kathleen Abadie[1,7], Arjun J. Kumar[1,2,7], **Pei Hsuan Wu[1]**, Morgan C. Jones[3], Nelli Aydinyan[3], Oren Barboy[4], Florence Chardon[5], Sriram Pendyala[5], Douglas M. Fowler[5], Ido Amit[4], Shivani Srivastava[6], Thelma M. Escobar[3], Hao Yuan Kueh[1, *]

3.1 Abstract

$CD8^+$ T cells differentiate into different terminal fates depending on the context of infections. In an acute infection, $CD8^+$ T cells differentiate into terminal effector cells; in a chronic infection, they differentiate into terminal exhausted cells. Albeit two separate fates, both silenced pro-memory genes, such as *Tcf7*, to uphold their commitments to terminal fates, suggesting a commonality in regulation between terminal effector and terminal exhausted differentiation. However, how and what are involved in upholding mechanisms in differentiation commitments is unclear. Using a previously developed *in vitro* assay that recapitulates the progression of naive T cells into terminal states, with stable silencing of *Tcf7*, we elucidated the mechanisms involved in maintaining terminal fates through cell-state-specific experiments. Previous cell state-specific Cas9 knockout screens found that the maintenance of *Tcf7* silencing required both Polycomb

Repressive Complexes (PRC) 1 and PRC2. Using CUT & RUN, we found that PRC1 and PRC2 established broad, heritable H3K27me3 and H2AK119ub1 domains at many pro-memory genes, such as *Tcf7,* to maintain their terminal states. As *Tcf7*+ "stem-like" precursor exhausted cells fuel the persistence of $CD8^+$response in a chronic setting and are the primary population to respond to checkpoint inhibitors, we investigated the effects of Polycomb inhibition to reprogram *Tcf7*- terminal exhausted cells into a *Tcf7*+ stem-like state. Terminal exhausted cells treated with Polycomb *Ezh2* inhibition during rest were able to reactivate *Tcf7* by preventing PRC2 maintenance of H3K27me3 and allowing passive dilution of H3K27me3 with cell divisions. The dissolution of H3K27me3 facilitates the transition of a closed, silenced chromatin state to an open active state, leading to the reactivation of *Tcf7.* This reactivation is independent of H2AK119ub1 dissolution, highlighting the differences in the mechanisms of repression of H3K27me and H2AK119ub1.

3.2 Introduction

While terminal effector and terminal exhausted T cells are two lineages arising from different infection contexts (acute vs chronic), both populations share many features throughout their differentiation and represent a terminal state. Upon TCR engagement and other inflammatory signals, both populations express common transcription factors, such as *T-bet, BLIMP-1,* and *IRF4*, which promote effector differentiation[32,34,35]. However, continuous TCR stimulation promotes the sustained and robust expression of transcriptional factors, such as *Tox*, a master regulator that further drives exhaustion differentiation[36,37]. On the other hand, as both populations progressed through their differentiation, they silenced memory-related transcription factors such as *Tcf7*[38–40], limiting their self-renewal and stem-like properties. While *Tcf7*+ precursor exhausted

cells are responsible for persistent responses in chronic infection and are the primary population expanding in response to immune checkpoint blockade, terminal exhausted T cells silenced *Tcf7,* leading to diminished tumor control. In an acute infection, terminal effector cells die with infection clearance, while in a chronic infection, terminal exhausted T cells remain exhausted, bearing an "epigenetic scar" of exhausted T cells even after stimulation withdrawal[41,42]. The commonality between the progression of terminal effector and exhausted lineages and their end cell-fate states suggests a shared mechanism in sustaining terminal T cell differentiation.

Due to its complexity, the impact of chromatin state on transcription and cell fate is an active field of research. Amongst chromatin regulation, the Polycomb repressive complexes (PRC) 1 and 2 play a crucial role in shaping the epigenetic landscapes, particularly during cell differentiation in mammalian development, where they maintain the repression of cell-type-specific genes[43,44]. PRC1 and PRC2 are histone-modifying complexes that are formed through multiple subunits. PRC1 includes two major classes, the canonical PRC1 (cPRC1) and variant PRC1 (vPRC1). The cPRC1 consists of the catalytic subunit (RING1a/b), a chromobox (CBX2,4,6,7,8) capable of reading H3K27me3, a polycomb group protein a (PCGF2,4) and a polyhomeotic homolog family protein (PHC1,2,3)[45,45,46]; while the vPRC1 does not have a CBX protein but instead contains RYBP/YAF-2 capable of reading H2AK119ub1[46,47]. Like PRC1, PRC2 is made up of subunits, consisting of catalytic subunits (EZH2), a H3K27me3 reader (EED), a scaffold (SUZ12), and RB binding protein, (RBBP4,7)[48].

PRC1 and PRC2 maintain broad domains of repressive markers by depositing H2AK119ub1 or H3K27me3, respectively. The current hierarchical model proposes that as PRC2 is initially

recruited to gene promoters, where it deposits the repressive histone mark H3K27me3. This mark is then recognized by the CBX protein within the cPRC1, leading to the recruitment of cPRC1 to the same genome loci. Once recruited, cPRC1 catalyzes H2AK119ub1. Furthermore, the EED subunit of PRC2 binds to existing H3K27me3, promoting further H3K27me3 deposition and enabling spreading of the repressive mark in nearby regions [49,50]. This broad repression domain established by PRC1 and 2 can silence genes in several ways, including chromatin compaction mediated by H3K27me3 or the PHC protein of cPRC1, blocking additional chromatin remodeling proteins or interfering with RNA Polymerase II activity[51]. However, the precise mechanisms underlying repression remained unclear. While PRC2 has been implicated in T cell differentiation, its role is not clearly defined; increased H3K27me3 deposition is observed at memory genes in terminal effectors mediated by the PRC2 methyltransferase subunit *Ezh2*[52]*;* however, *Ezh2* deletion could also enhance effector function or increase dysfunctions[50,53]. The conflicting findings resulting from different infection models and temporal deletions highlight the importance of uncovering the role of PRC2 in various environments. Additionally, whether PRC1 plays a role in terminal T cell differentiation and how PRC1 and PRC2 work together to drive terminal differentiation is also unclear.

Previous work using CRISPR screens done in the lab has identified PRC1 and 2 as crucial components in maintaining the silencing of *Tcf7* in terminal cells. In order to study the role of PRC1 and 2 in terminal T cell states, we used a minimal *in vitro* T cell exhaustion assay previously developed to generate various T cell states along the differentiation lineages defined by the states of their *Tcf7* and inhibitory receptor, *Tim3*: from stem-like or precursor state (T_{PRE}, *Tcf7*$^{+}$TIM3^{-}) to an intermediate (T_{INT}, *Tcf7*$^{-}$TIM3^{-}) and then terminally exhausted state (T_{TERM}, *Tcf7*$^{-}$TIM3^{+})

where self-renewal potential is lost. We then performed CUT & RUN in collaboration with the Escobar lab to profile the epigenetic states of naive T cells, T_{int}, T_{Term} and their persistence in T_{Term} after stimulation removal. Through chromatin profiling, we find that PRC1 and PRC2 work together to uphold commitment to a terminally state by depositing H3K27me3 and H2AK119ub1 and silencing many pro-memory genes, including *Tcf7*. We further show that Polycomb *Ezh2* inhibition, during stimulation withdrawal, inhibits *Ezh2* from maintaining H3K27me3 levels, allowing H3K27me3 to passively dilute with each cell division to reactivate *Tcf7* expression. Interestingly, the reduction in H3K27me3 did not impact H2AK119ub1 levels, suggesting that alternative models, besides the hierarchical model, are at play to maintain H2AK119ub1 independently of H3K27me3. Additionally, the loss of only H3K27me3 can reactivate *Tcf7***,** suggesting a difference in the repression mechanisms of H3K27me3 and H2AK119ub1.

3.3 Results

3.3.1 PRC1 and PRC2 Cooperatively locked down Memory loci in Terminally Differentiated CD8⁺ Cells

Precise gene regulations are essential for cell development and differentiation, with the chromatin and histone modifications playing a fundamental part in gene regulation. PRC1 and PRC2 have demonstrated how chromatin can influence gene regulation through their ability to establish broad repressive domains associated with gene silencing. As terminal $CD8^+$ T cells bear distinct transcriptional programs, silencing many memory-related genes, we wonder about the role of PRC1 and 2 in the commitment of terminal states. To investigate the role of PRC1 and PRC2 in the progression of $CD8^+$ T cell differentiation and fate commitment, we performed CUT&RUN on T cells in different differentiation stages: naive (d0) $CD8^+$ T cells, intermediate state (d2) (T_{INT},

Tcf7^{-}TIM3^{-}) and then terminally exhausted state (d6) (T_{TERM}, *Tcf7*$^{-}$TIM3^{+}) generated from our *in vitro* exhaustion system. Additionally, to probe whether these epigenetically modified states persist upon removal of stimulations, T_{TERM} cells were further rested for 8 days (d14). T cells were stimulated with proinflammatory cytokines, IL-12 or IFN-α, to promote different terminal differentiation; with IL-12 known to promote terminal cytotoxic effector cells, and IFN-α to promote exhaustions[54,55]. Previous experiments in the lab have also shown IL-12 stimulated cells biased terminal effector phenotype with reduced *Tox* levels, while IFN-α favored terminal exhausted state with sustained *Tox* expression.

While T-cells stimulated in either IL-12 or IFN-α showed similar Polycomb changes at the global level, they also showed notable histone modification differences at specific genes, consistent with these cells entering distinct terminal states **(Fig. 3.1)**. T-cells stimulated with IL-12 showed greater H3K27me3 deposition at exhaustion-associated genes (*Tox* and *Cd101*) and interferon-stimulated genes (e.g. *Ifit1, Ifi207*) compared to those stimulated with IFN-α (**Fig. 3.1B**). These results agreed with what was previously observed, where IL-12 downregulates *Tox* and directs cells towards terminal effector versus terminally exhausted fates. Furthermore, we performed Gene Set Enrichment Analysis (GSEA) to compare differentially H3K27me3-marked genes in IL-12 against gene signatures of short-lived effector cells in acute infection and terminally exhausted cells in chronic infection[56]. We found that genes preferentially methylated in IL-12 are expressed in exhaustion modules **(Fig. 3.1 C-D)**. These results are consistent with previous data and literature and suggest that IL-12 may epigenetically silence *Tox* expression and exhaustion gene programs to favor short-lived effector fates, whereas IFN-α favors exhaustion gene expression and drives exhaustion.

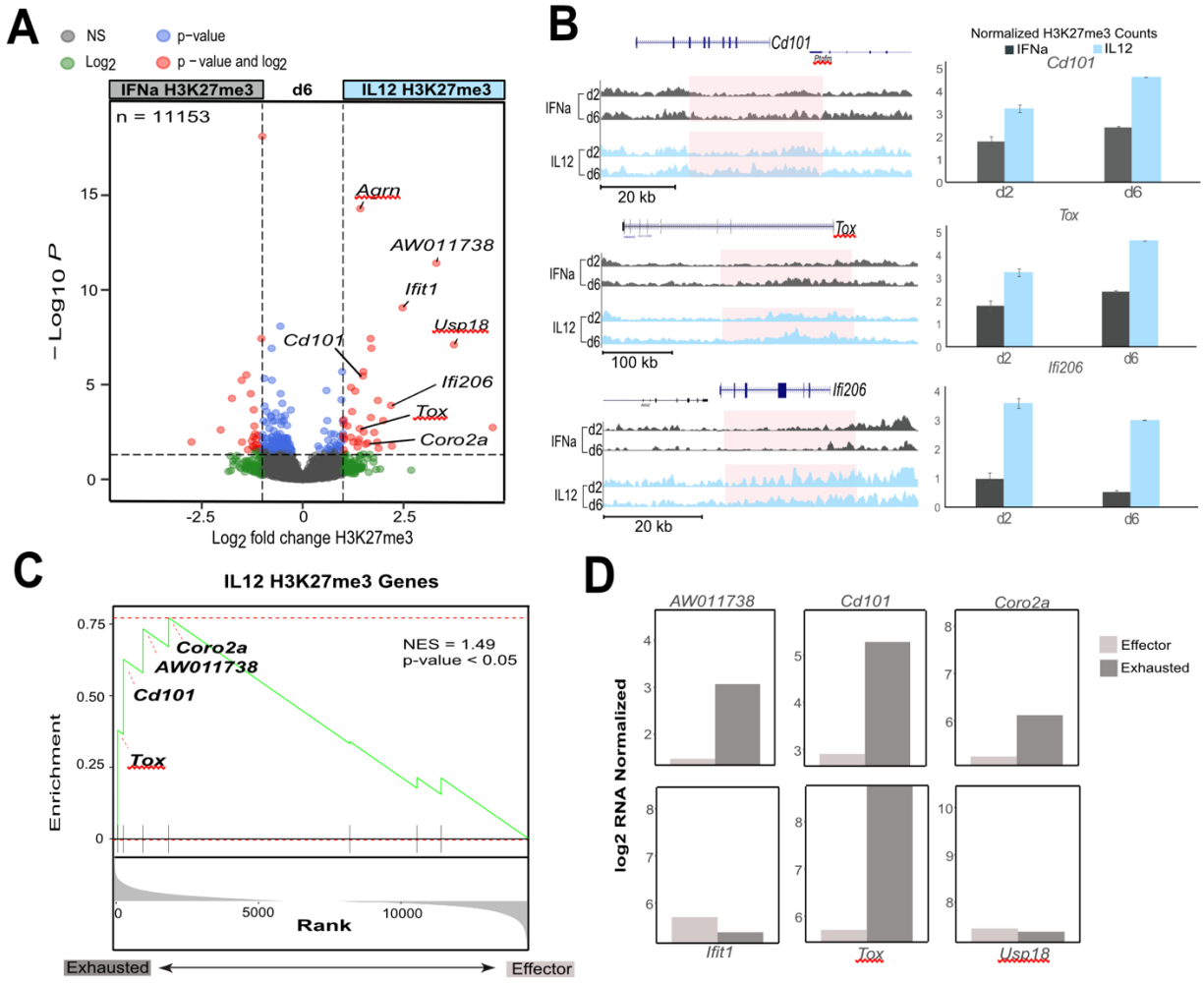

Figure 3.1. ***T-cells stimulated by IL-12 preferentially gain H3K27me3 modifications at exhaustion-associated gene loci.*** **(A)** Volcano plot shows genes with differential deposition of H3K27me3 in IFN-α (left) vs IL-12 (right. **(B)** Genome-browser tracks (left) showing H3K27me3 at *Cd101*, *Tox* and *Ifi206* for T-cells stimulated in IFN-α (gray) versus IL-12 (light blue) over two days (d2 and d6); bar plots (right) show normalized H3K27me3 counts within the pink shaded region highlighted (left). Error bars represent mean and standard deviation of two independent replicates. **(C)** Gene set enrichment analysis was performed using a custom set of genes differentially H3K27me3 modified in IL-12 across multiple timepoints (see Methods). Gene set enrichment plots compare the expression of genes in this gene set in exhausted cells (T_{EX}) versus short-lived effector cells (T_{EFF}) from acute and chronic LCMV infection[56]. **(D)** Normalized RNA counts of selected genes in this gene set in these T_{EFF} (light gray) versus T_{EX} (dark gray) populations[56]. This analysis shows that genes differentially H3K27 methylated upon IL-12 stimulation show elevated expression in terminally exhausted cells compared to effector cells. This suggests that IL-12 silences these genes to promote terminal effector lineages instead of terminally exhausted lineages.

On a global scale, extensive chromatin remodeling was seen as cells transitioned from naive T cells (d0) to T_{INT} upon TCR stimulation, occupying two distinct principal component spaces (PCA) **(Fig 3.2 C)**. A smaller shift was observed as cells transitioned from T_{INT} (d2) to T_{TERM} (d6), clustering closely together and far from naive cells. This shift away from d0 cells persisted for d14 cells, suggesting the similarities between d14 and d6 cells and the stable maintenance of epigenetic landscapes even after antigen withdrawal. The same trends were observed for both IL-12 and IFN-α, indicating a convergence in mechanisms for commitment to terminal fates and the persistence of their epigenetic states even after stimulation withdrawals **(Fig 3.2 C)**.

Next, to identify which genes stably gain or lose Polycomb modifications during T_{Term}, differentiation, we clustered genes based on their H3K27me3 and H2AK119ub1 distributions around their transcription start sites (TSS) (**Fig. 3.2D, Fig. 3.2A)**, with the focus on terminal exhausted cells. We found that a group of memory-related genes (*Bach2, Ccr7, Cd7, Id3, Lef1, Sell* and *Tcf7*) stably gained both H3K27me3 and H2AK119ub1 near their TSS upon differentiation that continued to remain after stimulation withdrawal (d14) (C1, **Fig. 3.2D; Fig. 3.2A**). The establishment of H3K27me3 domain aligned closely with the H2AK119ub1, indicating a cooperative coupling between PRC1 and 2.

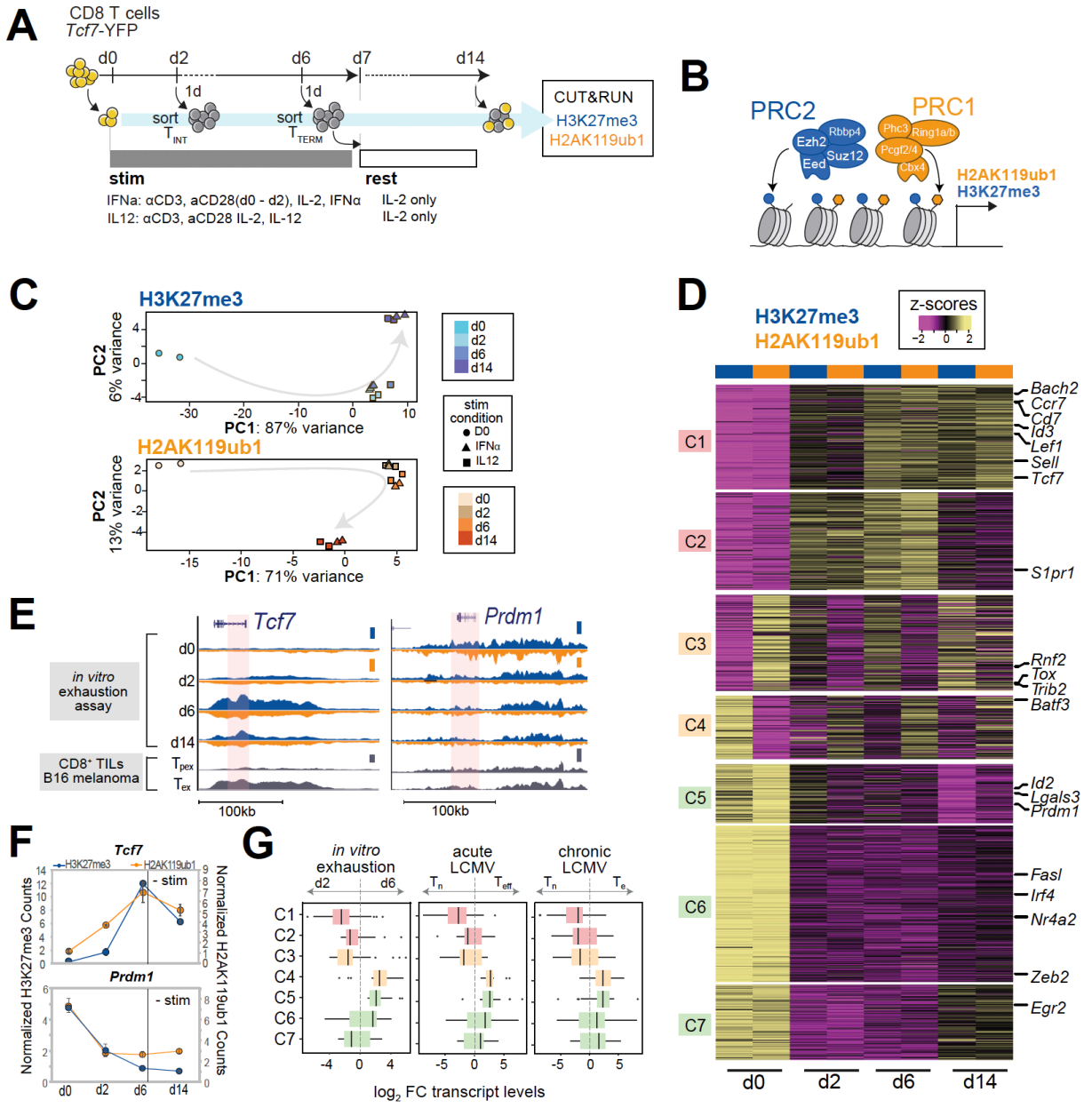

Figure. 3.2. ***PRC1 and PRC2 establish stable repressive chromatin domains at memory gene loci during terminal differentiation***. **(A)** Experimental overview. Resting CD8^{+}T-cells isolated from *Tcf7*-YFP reporter mice were subject to stimulation with IFN-α or IL-12 as indicated, then sorted for T_{INT} (*Tcf7*$^{-}$TIM3^{-}) or T_{TERM} (*Tcf7*$^{-}$TIM3^{+}) at the indicated timepoints. Sorted T_{TERM} were then re-cultured under resting conditions as indicated. Cells were then harvested at different timepoints (d0, d2, d6 and d14) for analysis of H3K27me3 and H2AK119ub1 genomic distributions using CUT&RUN. Plots in (D)-(F) show results of stimulation with IFN-α. **(B)** Schematic shows PRC1 and PRC2 along with the histone modifications they deposit. (**C**) Principal components analysis plots show H3K27me3 (top) and H2AK119ub1 (bottom) genomic distributions along the first two principal components, over all time points and inflammatory contexts. **(D)** Heatmap shows normalized H3K27me3 and H2AK119ub1 levels at the TSSs of all

genes showing differential levels of both modifications over time (fold-change > 2, p-adj < 0.05). Genes are partitioned into seven clusters (C1-C7), each with different temporal profiles of the two modifications. **(E)** Genome browser tracks show H3K27me3 (blue) and H2AK119ub1 (orange) distributions at *Tcf7* and *Prdm1* for *in vitro* exhausted CD8$^+$T-cells, as well as H3K27me3 (gray) distributions at the same loci for precursor (T_{PRE}) and terminally exhausted (T_{TERM}) tumor-specific CD8$^+$T-cells from B16 melanoma tumors[57]. Vertical bars indicate y-axis normalized scaling for corresponding histone modifications (*Tcf7*: H3K27me3: 0-15, H2AK119ub1: 0-15, B16 H3K27me3: 0-25; *Prdm1:* H3K27me3: 0-15, H2AK119ub1: 0-20, B16 H3K27me3: 0-15). **(F)** Normalized H3K27me3 and H2AK119ub1 counts at different time points within the highlighted regions in (E). Data represent mean and standard deviation of two independent replicates. **(G)** Bar charts fold changes (FC) in expression of genes from indicated clusters, between the pairs of T-cell populations indicated. Gene expression are obtained from profiling of *in vitro* exhausted cell populations(left; d2: cells stimulated for 2 days in IFNa and d6: cells stimulated for 6 days in IFNa), or from analysis of naive (T_N) effector (T_{EFF}) or terminally exhausted (T_{TERM}) subsets from acute and chronic LCMV infection[56].

Additionally, the H3K27me3 and H2AK119ub1 depositions were selectively downstream of the TSS **(Fig 3.2 D, E)**, consistent with the observed preferential H3K27me3 accumulation in the gene bodies of genes lacking transcription[58]. Furthermore, the H3K27me3 domain observed in our *in vitro* system was also seen in terminal exhausted (PD1+TIM3+) CD8$^+$T-cells in the B16 melanoma model[57] **(Fig 3.1 E-F)**, suggesting that the same Polycomb mechanism in silencing *Tcf7* happens in the tumor environment. Notably, the H3K27me3 and H2AK119ub1 domains around *Tcf7* spanned ~150kb **(Fig 3.2 E)**, highlighting the spreading of H3K27me3 markers, which have been implicated in facilitating PRC1 recruitment and looping of chromatin to repress gene expression[59]. Interestingly, a separate group of genes acquired H3K27me3 and H2AK119ub1 but lost them upon rest, showing that not all genes are involved in the epigenetic scarring of terminal exhausted states and maintained by PRC1 and 2 (C2, **Fig. 3.2D; Fig. 3.3A-B).** *S1pr1,* a gene involved in T cell migration, belongs to this cluster.

While *Tcf7* and other memory genes gained Polycomb domains during differentiation, a group of effector or exhaustion-promoting genes (e.g., *Prdm1, Irf4, Fasl, Zeb2, Egr2*) initially marked with

H3K27me3 and H2AK119ub1 lost both modifications upon differentiation (C5-6, F**ig. 3.2D; Fig. 3.3A)**. Similar to *Tcf7*, those that lost H3K27me3 and H2AK119ub1, such as *Prdm1,* also initially contained broad Polycomb domains, but subsequently lost both modifications downstream of TSS upon differentiation. The preferential loss of polycomb domain downstream of TSS in these clusters' points to a coupling between RNA-Polymerase and de-methylation of the genes, leading to gene upregulation **(Fig 3.3 D-E)**. These results suggest that the Polycomb system may repress the expression of effector regulators early to prevent premature differentiation but maintain the silencing of memory-like genes later to lock down terminal differentiation. It also implies that the effects of Polycomb inhibition may be state-dependent, offering insights into the conflicting results previously reported in the literature. Intriguingly, some genes were initially marked only with H3K27me3 (e.g., *Batf3* in C4) or H2AK119ub1 (e.g., *Tox* and *Trib2* in C3) **(Fig. 3.1D)**. These singly modified states suggest that PRC1 and PRC2 can work independently at some genomic loci.

To directly test whether Polycomb domain formation is associated with silencing and whether Polycomb domain dissolution is associated with activation of effector genes, we examined whether genes that gained or lost H3K27me3 and H2AK119ub1 modifications (C1-C7) also showed gene expression changes, in our in vitro assay comparing acute and chronic stimulated cells, or upon differentiation from a naive (T_N) to a terminal effector (T_{EFF}) or exhausted state (T_{EX}) during LCMV infection[56] **(Fig. 3.1G)**. Genes gaining both H3K27me3 and H2AK119ub1 were down-regulated upon differentiation across all three contexts (C1, C2), with stronger down-regulation observed for genes irreversibly gaining both modifications (C1). Additionally, genes that lost both H3K27me3 and H2AK119ub1 upon stimulation increased in expression during differentiation (C5-C7), with greater up-regulation observed for genes that irreversibly lost these modifications

(C5). These findings link stable Polycomb domain formation (or dissolution) to the silencing of memory genes (or activation of effector genes) during differentiation.

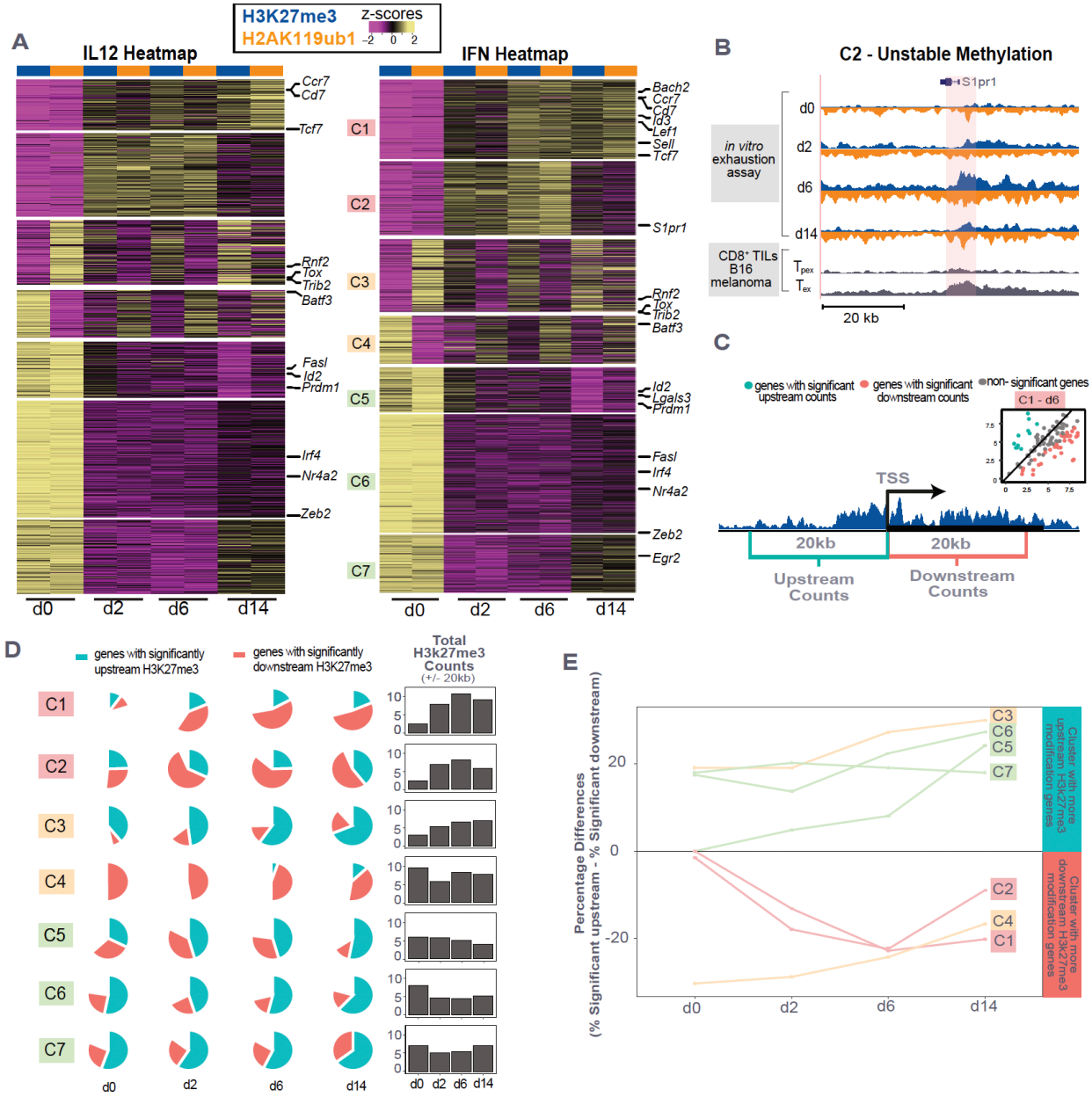

Figure 3.3. ***Genome-wide analysis of H3K27me3 and H2AK119ub1 dynamics and stability during terminal T-cell exhaustion in our in vitro system***. **(A)** Heatmap of normalized counts in H3K27me3 and H2AK119ub1 differentially modified regions (fold-change > 2, p adj < 0.05) for d0, d2, d6 and d14 cells stimulated in IL-12 (left) and IFN-α (right). **(B)** Genome-browser tracks showing both H3K27me3 (blue) and H2AK119ub1 (orange) distributions at *S1pr1* from T-cells undergoing *in vitro* exhaustion differentiation, as well as H3K27me3 (gray) distributions at the same locus from tumor-targeting T_{PRE} and T_{TERM} populations (from Ford et al 2022[57]). **(C)** Scheme

to identify genes with preferential enrichment of H3K27me3 either upstream (teal) or downstream (red) of their TSS. Scatterplot example (inset) shows upstream against downstream H3K27me3 counts for single cluster (C1) and timepoint (d6). Genes with statistically significant H3K27me3 enrichment upstream or downstream of the TSS were identified (see Methods). **(D)** Pie charts (left) show percentage of genes with preferential significant upstream or downstream H3K27me3 marks (fold-change>1.2, pval<0.01) for each cluster across d0, d2, d6 and d14. Bar plots (right) show average total H3K27me3 counts over time over all genes within the indicated cluster. **(E)** Plots show percentage differences of genes showing preferential enrichment of H3K27me3 upstream versus downstream of their TSSs. This analysis suggests that genes gaining H3K27me3 preferentially gain this modification downstream of their TSS (C1, C2), whereas genes losing H3K27me3 preferentially do so downstream of their TSS (C5, C6).

3.3.2 Tazmetostat restores Tcf7 expression by inhibiting active maintenance of H3K27me3 levels by PRC2 across cell divisions

The CUT&RUN data suggested PRC1 and PRC2 jointly deposit H3K27me3 and H2AK119ub1 at the *Tcf7* locus and other memory gene loci, cooperating to maintain the silencing of stem-like genes and upholding terminal differentiation commitment. We hypothesized that PRC2 inhibition can reverse the stable repressive chromatin domains established in T_{TERM} cells and drive *Tcf7* reactivation. To test this hypothesis, we generated T_{TERM} cells and subsequently rested them without stimulation, in the presence of IL-15, a cytokine that has been shown to play a crucial role in homeostasis proliferation, and survival of memory $CD8^+$ T cells[60]. We targeted PRC2 Ezh2 subunit using small molecule inhibitor, Tazmathestat (Taz). We then measured *Tcf7-YFP*, and H3K27me3 levels using flow cytometry at 0, 24, 48, 72 hrs after rest **(Fig 3.4A)**.

In the absence of an inhibitor, T_{Term} maintained *Tcf7-YFP* negative for the first 2 days of rest, with only 11.9% of cells able to reactivate *Tcf7-YFP* by day 4 of rest. In contrast, 38.2% of Taz-treated cells reactivated *Tcf7-YFP* by day 4 **(Fig. 3.4B)**. Given that Taz targets the H3K27me3 catalytic subunit of PRC2, Ezh2, we expect Taz-treated cells to have a decrease in their H3K27me3 levels. As expected, while non-Taz-treated cells maintained their H3K27me3 levels throughout divisions,

consistent with the fixed epigenetics observed in exhausted T cells (**Fig. 3.4 C, D),** Taz-treated cells showed a reduction in H3K27me3 with cell divisions **(Fig. 3.4 D,E)**. Together, they suggested the active role PRC2 played in maintaining H3K27me3 in terminal exhausted cells and by preventing PRC2 from upkeeping the H3K27me3 level, *Tcf7-YFP* was able to reactivate.

It is unclear whether *Tcf7* reactivation occurs concurrently with H3K27me3 reduction or whether it happens in a stepwise manner, reactivating only after certain H3K27me3 levels are reached, with the additional repressive mechanism being unlocked. Furthermore, the loss of H3K27me3 could be due to either other enzymatic removal of the marks or the dilution of parental modification over cell divisions. Therefore, we proposed two models **(Fig 3.4F)** for Taz-mediated H3K27me3 reduction and *Tcf7* reactivation. The first model suggested H3K27me3 is removed by demethylase, reactivating *Tcf7* concurrently, while the second model proposed passive dilution of H3K27me3 and unlocking additional repressive mechanisms are required for *Tcf7* reactivation. To test whether the loss of H3K27me3 is due to passive dilution, we plotted the levels of H3K27me3 left against cell divisions **(Fig 3.4 G)** for both cells treated with and without Taz**.** If H3K27me3 is passively diluted with cell division, 50% is lost with each cell divisions[61]. While cells without Taz only lost 20% of their H3K27me3 with cell divisions, cells treated with Taz lost 45% of H3K27me3 with each cell division, consistent with the passive dilution model of H3K27me3 **(Fig 3.4 G)**. This suggested that while Taz prevented the active maintenance of H3K27me3 by PRC2, cell divisions are required to reduce H3K27me3 levels for *Tcf7* reactivation. Notably, *Tcf7* reactivation only occurred when H3K27me3 reached a certain level at d2, suggesting that the reduction in H3K27me3 may facilitate transcription initiation in a stepwise manner. Consistent with these

results, *Tcf7* positive cells did not display a lower H3K27me3 level than *Tcf7* negative cells after the same amount of resting **(Fig. 3 .4H)**.

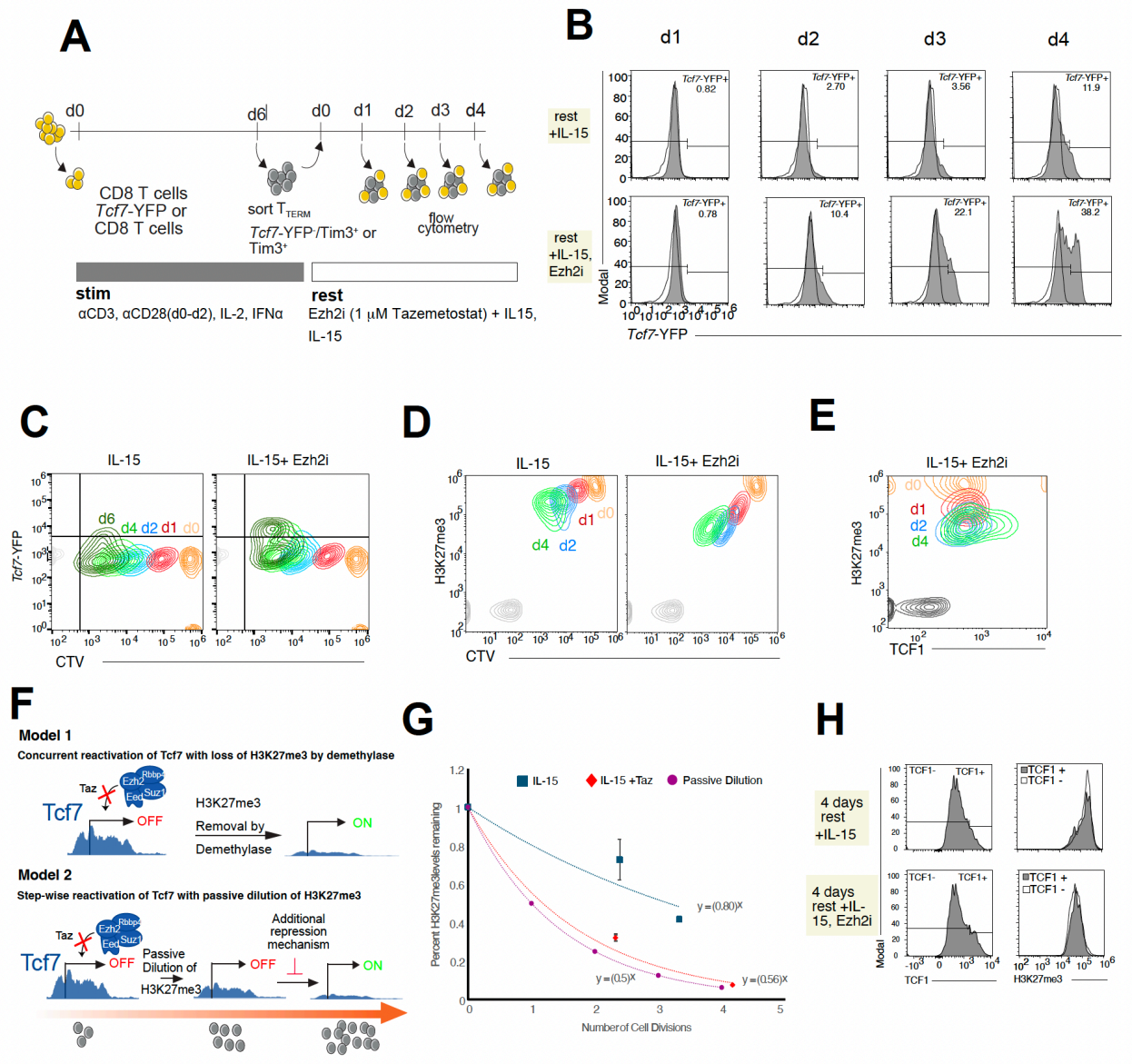

Figure 3.4. ***Polycomb inhibition prevents active maintenance of PRC2 and allows passive dilution of H3K27me3 to reactivate Tcf7.*** **(A)** Experimental overview. CD8+T-cells from *Tcf7-YFP* or P14 mice were chronically stimulated for 6 days as described before in the presence of IFN-α. They were then sorted for T_{TERM} and transferred to the resting conditions (IL-15 with or without Ezh2 inhibitors). Cells were analyzed by flow cytometry at days 0,1,2,3,4. **(B)** T_{TERM} cells were cultured at rest in a combination of indicated drugs and cytokines, then analyzed by flow cytometry for *Tcf7*-YFP expression. (**C)** T_{TERM} cells were stained with CTV and cultured at rest in

the combination of indicated drugs and cytokines, then analyzed by flow cytometry for CTV and *Tcf7*-YFP expression. **(D)** Flow plot showing overlaid d0, d1, d2, d4 H3K27me3 levels versus CTV in T_{TERM} treated with IL-15 or IL-15 with Ezh2 inhibitor. **(E)** Flow plot showing overlaid d0, d1, d2, d4 H3K27me3 levels versus TCF-1 levels in T_{TERM} treated with IL-15 with Ezh2 inhibitor. **(F)** Proposed mechanisms for loss of H3K27me3 and activation of *Tcf7*. **(G)** Graph plotting levels of H3K27me3 left against cell divisions for cells treated with IL-15 (blue), IL-15 with Taz (orange). The curves were compared to the passive dilution model (purple). **(H)** Histogram (right) showing H3K27me3 levels in TCF1 positive or negative population (left).

3.3.3 Reactivation of Tcf7 in cells treated with Tazemetostat is independent of H2AK119ub1 reduction

Current models propose that PRC2 subunit *Ezh2* deposits H3K27me3 to recruit the cPRC1 and promote H2AK119ub1 at target genomic loci. Additionally, PRC2 can recognize H3K27me3 to spread further and deposit H3K27me3. These feedback mechanisms and cooperation between cPRC1 and PRC2 enabled the broad establishment of repressive domains, which contain both modifications, thereby silencing gene expression. With the close collaboration between cPRC1 and PRC2, it is plausible that cells treated with Taz would impact the feedback between cPRC1 and PRC2 and the H2AK119ub1 levels. Additionally, whether the reactivation of *Tcf7* also depends on the reduction of H2AK119ub1 is unclear. To investigate the role of H2AK119ub1 in silencing *Tcf7*, we stimulated cells described above, rested in either IL-15 or IL-15 with Taz, and stained for H3K27me3 and H2AK119ub1 **(Fig 3.5B).**

Globally, cells gained H3K27me3 and H2AK119ub as they progressed through differentiation, and transitioned T_{TERM} (*Tcf7*$^{-}$TIM3^{+}) state (**Fig 3.5B, C).** The most significant increase of H3K27me3 and H2AK119ub1 was observed between d0 and d2**,** suggesting global chromatin remodelling upon TCR stimulation, consistent with the CUT&RUN data. Upon Taz treatment, we observed a decrease in global H3K27me3 levels, as expected from inhibition of Ezh2. However,

this decrease in global H3K27me3 levels was not accompanied by a concomitant decrease in global H2AK119ub1 levels. Instead, cells treated with Taz had similar H2AK119ub1 levels to those not treated with Taz **(Fig. 3.5B)**. However, as H3K27me3 reduction can still reactivate *Tcf7,* this suggests distinct repression mechanisms for PRC1 and PRC2.

The persistence of H2AK119ub1 in the absence of H3K27me is inconsistent with the proposed coupling of cPRC1 and PRC2 model. Additionally, the removal of H3K27me3 is sufficient to reactivate *Tcf7,* suggesting a difference in the mechanisms of repression by H3K27me3 and H2AK119ub1. While cPRC1 is thought to be recruited mainly through recognition of H3K27me3 through the Cbx subunit, in *Drosophila*, cPRC1 has been reported to bind independently of H3K27me3[62,63]. Furthermore, recent studies have shown that cPRC1 containing Cbx2, 7, 8 may occupy Polycomb target genes independently of H3K27me3 in embryonic stem cells, deviating from the proposed model of cPRC1 recruitment[64,65]. One mechanism observed showed that PRC1-condensed chromatin facilitated multivalent interactions, allowing the positively charged CBX8 of cPRC1 to bind to negatively charged DNA, modified or unmodified tails of histones[66]. These interactions provided multiple docking sites for cPRC1, allowing cPRC1 to dynamically move throughout and maintain a condensed yet accessible chromatin state independently of H3K27me3[66]. Similarly, cPRC1 can reorganize the 3D genome and establish chromatin compaction through polymerization of its PHC subunits, potentially keeping cPRC1 localized at repressive gene loci to maintain H2AK119ub1 levels. As the chromatin condensation has likely been established in the terminal exhausted cells, the spatial properties of the chromatin could potentially explain how cPRC1 can occupy and maintain H2AK119ub1 levels independently of

H3K27me3. **(Fig 3.5C).** The 3D spatial organization of the chromatin mediated by cPRC1 could also allude to how cPRC1 silences *Tcf7* independently of H3K27me.

Another possible explanation of how H2AK119ub1 is maintained in the absence of H3K27me3 is through the variant PRC1 (vPRC1) complex. vPRC1 is thought to be more catalytically active than cPRC1 and can be recruited to the site independently of H3K27me3. Instead, vPRC1 recognizes H2AK119ub1 and further catalyzes H2AK119ub1 deposition[67]. As vPRC1 and cPRC1 shared many subsets of target[64,68], vPRC1 may have compensated for cPRC1 activity, maintaining the levels of H2AK119ub1 despite the reduction in H3K27me3 levels **(Fig 3.5C).**

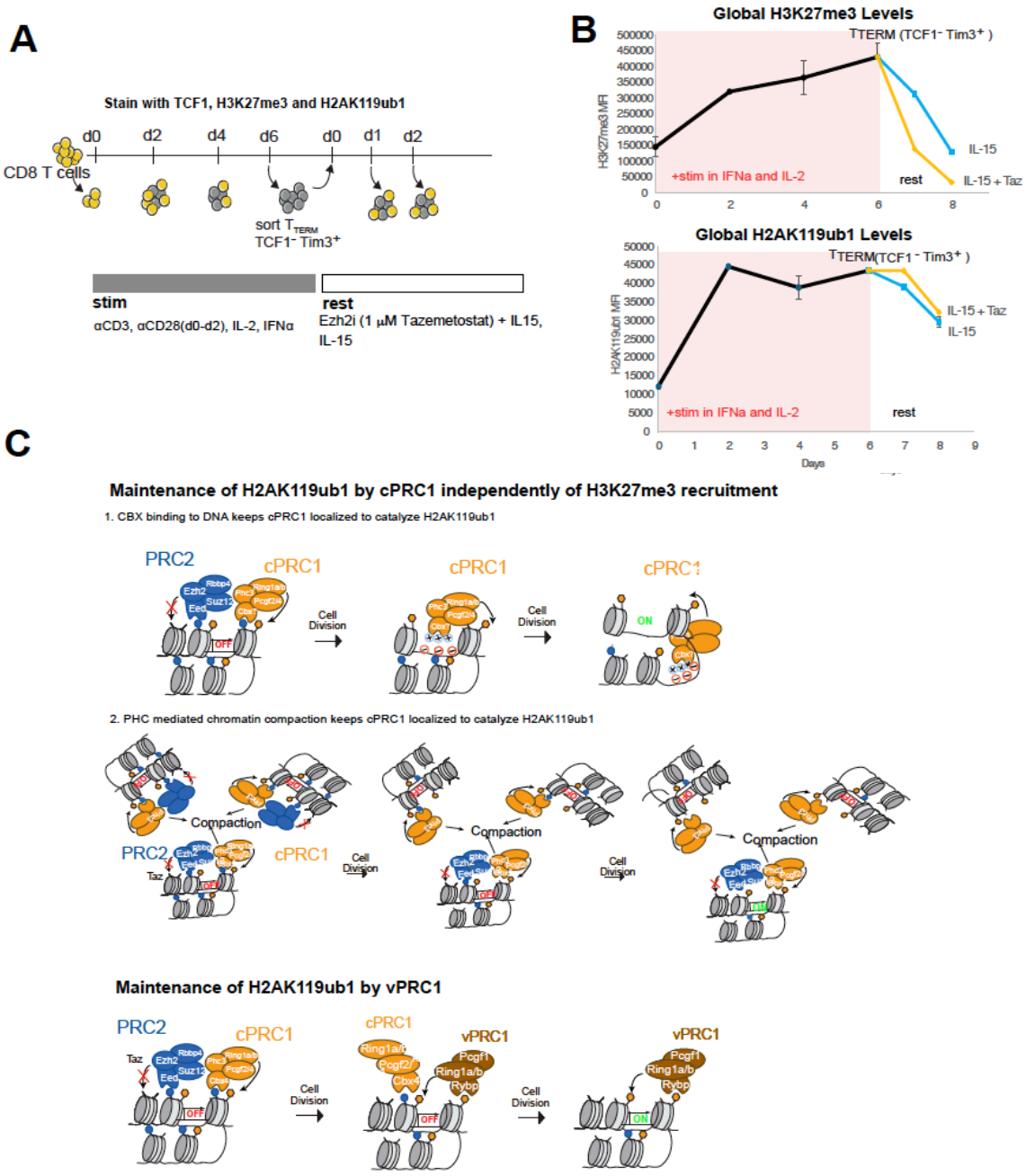

Figure 3.5. ***Maintenance of H2AK119ub1 in cells treated with Tazemetostat.*** (A) Experimental overview. (B) MFI of H3K27me3 and H2AK119ub1 levels throughout stimulation and rest in IL-15 (blue) or IL-15 + Taz treatment (orange). (C) The proposed models of the role of cPRC1, vPRC1 and PRC2 played in maintaining H2AK119ub1 in terminally exhausted cells rested in IL-15 and Taz. Model 1 proposed condensed chromatin allowed cPRC1 to localize at repressive loci independently of H3K27me3 to maintain H2AK119ub1 levels. Model 2 proposed the compensation of cPRC1 with vPRC1 to maintain H2AK119ub1 levels.

3.3.4 Tazmetostat-treated cells promote stem-like phenotypes

As *Tcf7* expression can be associated with stemness and quiescence[40], we next investigate if the phenotypes of Taz-treated cells showed increased stem-like and decreased exhaustion phenotypes. Cells were stained for PD-1 and CD62L and analyzed with flow cytometry. The levels of PD-1 correspond with the levels of exhaustion; specifically, a high PD-1 population is associated with dysfunction and a poor clinical prognosis compared to a low PD-1 population[69], while CD62L is linked to memory and stem-like cells[70]. The PD-1 levels of Taz-treated cells decreased significantly more compared to IL-15 during d2-d4 of rest, displaying restoration of exhaustion in Taz-treated cells. Furthermore, Taz-treated cells also expressed a higher level of CD62L, a cell surface marker associated with naive and memory cells[71], than those in IL-15, suggesting a more stem-like phenotype. These findings showed that Taz-treated cells exhibit a phenotype consistent with stem-like cells, with a reduced exhaustion phenotype observed.

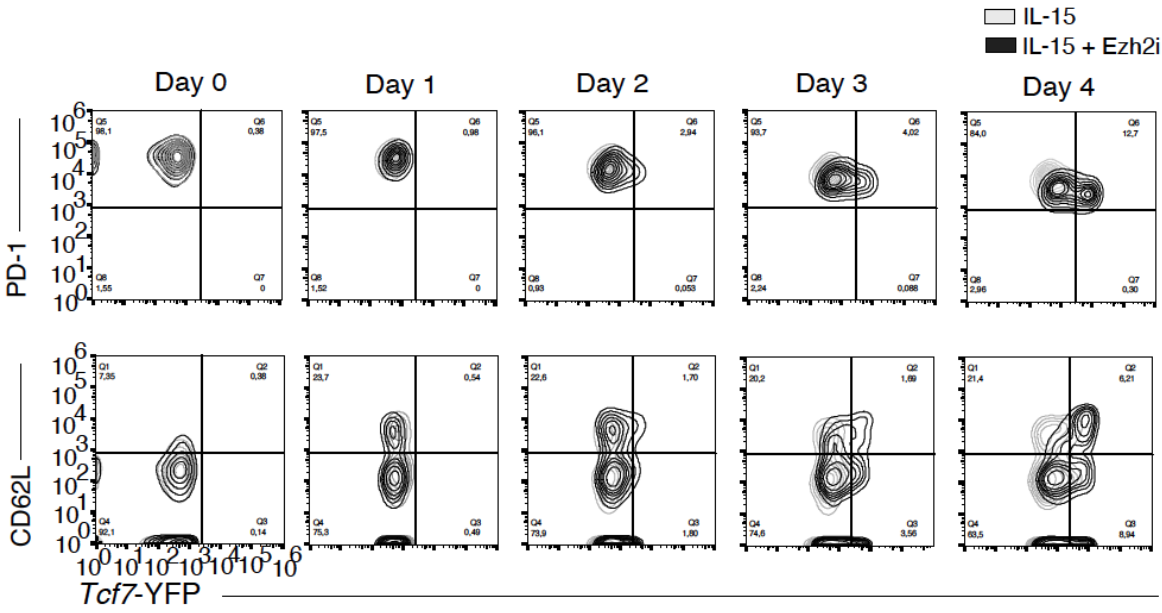

Figure 3.6. ***Polycomb inhibition promotes a stem-like state.*** Flow chart showing PD-1 and CD62L expression from d0 - 4 in T_{TERM} treated with IL-15 (light grey) or IL-15 with *Ezh2* inhibitor (black).

Discussion

Terminally exhausted T cells are dysfunctional and fail to eliminate chronic viral infections or cancers, with distinct epigenetic states that remain even after clearance of threats. However, the epigenetic mechanisms of T cell exhaustion remain unclear, with potential for reprogramming terminally exhausted T cells into more stem-like exhausted precursors capable of eliminating chronic threats.

First, we show that PRC 1 and 2 played a role in upholding T cells' commitment to terminal T cell fates. PRC1 and PRC2 are known to cooperate and form feedback loops that enable the formation and spreading of polycomb domains to repress gene expression. However, their roles and interactions have mostly been studied in embryonic stem cells, but not in mammalian $CD8^+$ T cells. Here, we showed that PRC1 and 2 established broad domains of H2AK119ub1 and H3K27me3 at many pro-memory gene loci, including *Tcf7*, highlighting a close co-operation between PRC1 and PRC2 to repress memory-related genes in terminally exhausted cells. These modifications were maintained even after stimulation withdrawal. Additionally, H2AK119ub1 and H3K27me3 domains were observed in effector and exhausted-associated gene loci early in differentiation but subsequently lost as cells progressed, highlighting the dual roles of PRC1 and 2 in not only maintaining terminal fates but also in preventing premature differentiation of T cells. This finding offers new insights into how various temporal deletions of Ezh2 yielded different results previously in the literature.

Second, through Polycomb inhibition, we were able to reprogram terminally exhausted T cells into a more stem-like precursor state, characterized by the reactivation of *Tcf7*. As *Tcf7* is a transcription factor critical for cell stemness and memory, *Tcf7*+ exhausted T cells are associated

with better self-proliferation, persistent response and better clinical response during cancers. However, with current immunotherapies, such as checkpoint inhibitors, many are aimed at delaying terminal exhaustion but not preventing it, unable to solve the inevitable inability of dysfunctional exhausted T cells to clear off cancers. Here, we showed that with the Polycomb inhibition during rest, we were able to reverse the silencing of *Tcf7* in terminally exhausted T cells. The polycomb inhibitor, Tazmatostat, inhibits PRC2 writer, *Ezh2,* from actively maintaining the repressive chromatin, enabling the passive dilution of H3K27me3 with each cell division. Interestingly, the dissolution of H3K27me3 does not impact H2AK119ub1 levels, suggesting cPRC1 can work independently without PRC2 or vPRC1 compensating for cPRC1 and pointing to different repressive mechanisms, potentially involving the chromatin spatial arrangements[66,72]. Further work would need to be done to elucidate the underlying interactions and mechanisms between PRC1 and PRC2 involved in *Tcf7 repression* and reactivation.

Collectively, these data showed the crucial role and involvement of PRC1 and 2 in maintaining the epigenetic landscape of terminally exhausted T cells. The Polycomb inhibition points to novel therapeutic possibilities that could reprogram the epigenetics of exhausted T cells into a more stem-like state. However, it is unknown how inhibition of PRC1 and 2 would impact the cells' functional aspects. Additional functional and *in vivo* experiments would need to be performed to understand the functional potential of these reprogrammed cells.

3.5 Methods

Mice

All mice were used following the guidelines of the University of Washington Institutional Animal Care and Use Committee (approved protocol #4397-01). C57Bl/6J mice (Strain #000664) and P14 mice (Strain #004694) were purchased from the Jackson laboratory. *Tcf7*-YFP mice were a gift from Avinash Bhandoola (NIH)[73].

CD8$^+$T-cell isolation

Spleens were harvested and a single cell suspension of splenocytes was generated by manual dissociation between rough microscope slides and filtered over 50 µm nylon mesh. Red blood cells (RBC) were lysed for 3-5 minutes at room temperature using in house RBC lysis buffer (1 mM EDTA, 10 mM NaHCO3, 150 mM NH4Cl) and quenched with HBH flow buffer (HBSS + 0.5% BSA). Cells were resuspended in Fc blocking buffer (2.4G2 supernatant in HBH) and incubated on ice for 15-30 minutes. CD8$^+$T-cells were isolated by magnetic separation following the manufacturer's instructions with the CD8$^+$a+ T-cell isolation kit (Miltenyi #130-104-075).

Ex vivo CD8$^+$ T-cell differentiation

One day prior to T-cell activation, cell culture plates were coated with 1 µg/mL αCD3 (Cytek Clone: 145-2C11) and 0.5 µg/mL αCD28 (Cytek Clone: Clone: 37.51) in PBS and incubated overnight at 4°C. CD8$^+$T-cells were plated in 24 well plates with 0.1-2.5 E6 cells/mL in T-cell medium (TCM, RPMI 1640 + L-Glutamine (Gibco), 10% heat inactivated FBS (VWR), 1% Non essential amino acids (Gibco), 1% Sodium Pyruvate (Gibco), 2% 1M HEPES (Gibco), 1% Pen-Strep-Glutamine (Life Technologies) and 50 µM 2-Mercaptoethanol (BME, Sigma Aldrich)).

TCM was supplemented with 100 U/mL recombinant human IL-2 (Peprotech #200-02), and where applicable 1 μg/mL murine IL-12 (Peprotech #210-12), or 1000 U/mL murine IFN-α (Biolegend #752804). On days 2, and 4 of culture, 50% of the cells were harvested for flow cytometry analysis and the remaining 50% was plated into fresh stimulation plates. Cells were incubated at 37°C, 5% CO_2. For resting assays, cells were transferred to non-coated plates and cultured in 100 ng/mL IL-15 only unless otherwise noted in the figure caption. Where applicable, cells were stained following the manufacturer's instructions with 5 μm CellTrace Violet (ThermoFisher #C34557).

Flow cytometry, sorting, and intracellular staining

Cells were incubated in Fc blocking buffer for 10-15 minutes on ice, then stained with extracellular antibodies for 20 minutes on ice and resuspended in HBH buffer. Cells were analyzed on an Attune NxT (Thermofisher), or sorted on a FACS Aria II (BD, UW Genome Sciences) or FACS Aria III (BD, UW Pathology). Data analysis was performed with FlowJo (BD). Cells were centrifuged at 300g for 5 minutes and resuspended in Fc blocking buffer and incubated for 10-15 minutes on ice, then fixed and permeabilized in 4% paraformaldehyde (eBioscience Foxp3/Trascription Factor Staining) for 30 min on ice. Cells were rinsed 2x with Perm/Wash buffer then resuspended in the following antibodies at 1:100 dilution in Perm/Wash buffer: anti-H3K27me3(AF-488, Cell signaling #5499), anti-H2AK119ub1 (AF-488, Cell signaling #26498S), and anti-TCF1 (PE, Biolegned #7F11A10).

Small molecule inhibition of PRC1/2

Where applicable, cells were cultured in 1 μM EZH2i Tazemetostat (Selleckchem #S7128), 10 μM RING1i PRT4165 (MedChemExpress #HY-19817), or 0.1% DMSO.

Chromatin profiling by CUT&RUN

CUT&RUN assays were performed using the Epicypher CUTANA CUT&RUN kit (Epicypher 14– 048). Briefly, Cells were activated following ex vivo differentiation, described above. Sorted cells were fixed in a final concentration of 0.1% formaldehyde for 1 minute, quenched with glycine in a final concentration of 0.23M, then pelleted and frozen prior to downstream use. Thawed cells were then washed and incubated with concanavalin A beads (1:10) for 10 min followed by a wash sttep and then incubation in (0.01% digitonin) buffer with antibodies recognizing H3K27me3 (Cell Signaling 9733S) and H2AK119ub1 (Cell Signaling 8240S) overnight at 4°C. Cells were then washed in permeabilization buffer (0.01% digitonin), then incubated with pAG-MNase for 10 min at room temperature. pAG-MNase was then activated with CaCl2, with reaction allowing to proceed for 2 hrs 4°C before adding EDTA containing stop buffer (spiked with 0.5ng E.coli DNA) to quench. Un-crosslinking was then performed with the addition of proteinase K and SDS. Permeabilization buffer, Protein A–micrococcal nuclease (pA-MNase) was then added, followed by CaCl2 to cleave the antibody-bound chromatin. Enriched DNA was purified using magnetic beads provided by kit, then washed with 85% EtOH and isolated with 0.1x TE Buffer. Two replicates were performed for each antibody. Libraries were prepared using CUTANA library prep kit (Epicypher 14-1001) with the Illumina P2 100 Cycle Cartridge (Illumina 20044468) and flow cell (Illumina 2002770), and sequenced using an Illumina NextSeq 2000 (61bp cycles, with libraries pooled to a final concentration of 650pM).

CUT&RUN Data Pre-Processing. FastQC (v0.12.1) was used to perform quality assessments on all fastq files. Fastp (v0.23.4) was used to filter out low-quality reads (-q 30) and to trim the

polyG tail and adapters. The processed fastq files were aligned to mouse reference genome (GRCm38) using Bowtie2 (v2.4.2). Mitochondria reads and blacklisted regions were filtered out prior to peak calling using bedtools intersect.

Peak Calling. SEACR (v1.3) was used to call peaks for each sample against igG controls, using the norm, stringent settings. Bedtools intersect was used to select consensus peaks between replicates, followed by merging all peaks into a superset for each marks. FeatureCounts were used to count the reads within peaks for each samples.

Differential Peak Analysis. ChIPpeakAnno (v3.36.1) (Zhu et al 2010) was used to annotate peaks to the nearest genes[74]. Only peaks within 3kb of the promoter were used for DESeq2 (v1.42.1) analysis. DESeq2 was applied to raw counts for called peaks in a pairwise manner to determine the differentially modified regions defined by those with FDR (Benjamini-Hochberg) < 0.05 and a fold change > 2. The differential peaks were compiled into a master differential peaks list for each marks. Statistical analysis and visualization of sequencing data was performed using custom R scripts.

Track Generation. DeepTools bamCoverage (3.0.2) was used to convert bam files to bigwig files for visualization. The bigwig was normalized using the RPGC option.

Statistical analysis of H3K27me3 distributions at the TSS. Genes with H3K27me3 differentially modified region across the timepoints were used for the asymmetric analysis. Genes less than 20kb were filtered out. Genome coordinates associated with 20kb upstream and downstream of TSS were obtained using Rsurebread (v2.16.1). Raw counts within the range were obtained with FeatureCounts. Binomial test was conducted on the raw upstream and downstream

counts for each gene within each sample, with a null hypothesis that the proportion of upstream counts is equal to of downstream counts. The p value obtained were then adjusted using Bonferroni corrections. The same analysis was performed to determine genes with significantly downstream modifications. Genes were considered significantly enriched in H3K27me3 upstream/downstream if the fold change of upstream/downstream or downstream/upstream > 1.2 and q values < 0.01 for both the replicates.

Gene Set Enrichment Analysis for CUT&RUN. Gene Set Enrichment Analysis (GSEA) was performed using the Broad Institute software (https://www.broadinstitute.org/gsea/index.jsp). Custom gene sets were created using IL-12 differentially methylated genes on 2 or more days. The effector and exhausted dataset from Scott - Browne *et al.* (GSE88987) were compared and enrichment scores were visualized.

References

1. In brief: The innate and adaptive immune systems (2023). In InformedHealth.org [Internet] (Institute for Quality and Efficiency in Health Care (IQWiG)).

2. Andersen, M.H., Schrama, D., thor Straten, P., and Becker, J.C. (2006). Cytotoxic T Cells. J. Invest. Dermatol. *126*, 32–41. https://doi.org/10.1038/sj.jid.5700001.

3. Raskov, H., Orhan, A., Christensen, J.P., and Gögenur, I. (2021). Cytotoxic $CD8^+$ T cells in cancer and cancer immunotherapy. Br. J. Cancer *124*, 359–367. https://doi.org/10.1038/s41416-020-01048-4.

4. Nolz, J.C., Starbeck-Miller, G.R., and Harty, J.T. (2011). Naive, effector and memory $CD8^+$ T-cell trafficking: parallels and distinctions. Immunotherapy *3*, 1223–1233. https://doi.org/10.2217/imt.11.100.

5. Hoffmann, M.M., and Slansky, J.E. (2020). T cell receptor affinity in the age of cancer immunotherapy. Mol. Carcinog. *59*, 862–870. https://doi.org/10.1002/mc.23212.

6. van der Merwe, P.A., and Dushek, O. (2011). Mechanisms for T cell receptor triggering. Nat. Rev. Immunol. *11*, 47–55. https://doi.org/10.1038/nri2887.

7. Ganti, R.S., Lo, W.-L., McAffee, D.B., Groves, J.T., Weiss, A., and Chakraborty, A.K. (2020). How the T cell signaling network processes information to discriminate between self and agonist ligands. Proc. Natl. Acad. Sci. *117*, 26020–26030. https://doi.org/10.1073/pnas.2008303117.

8. McKeithan, T.W. (1995). Kinetic proofreading in T-cell receptor signal transduction. Proc. Natl. Acad. Sci. U. S. A. *92*, 5042–5046.

9. Voisinne, G., Locard-Paulet, M., Froment, C., Maturin, E., Menoita, M.G., Girard, L., Mellado, V., Burlet-Schiltz, O., Malissen, B., Gonzalez de Peredo, A., et al. (2022). Kinetic proofreading through the multi-step activation of the ZAP70 kinase underlies early T cell ligand discrimination. Nat. Immunol. *23*, 1355–1364. https://doi.org/10.1038/s41590-022-01288-x.

10. Kersh, G.J., Kersh, E.N., Fremont, D.H., and Allen, P.M. (1998). High- and Low-Potency Ligands with Similar Affinities for the TCR: The Importance of Kinetics in TCR Signaling. Immunity *9*, 817–826. https://doi.org/10.1016/S1074-7613(00)80647-0.

11. Altan-Bonnet, G., and Germain, R.N. (2005). Modeling T Cell Antigen Discrimination Based on Feedback Control of Digital ERK Responses. PLOS Biol. *3*, e356. https://doi.org/10.1371/journal.pbio.0030356.

12. Chen, L., and Flies, D.B. (2013). Molecular mechanisms of T cell co-stimulation and co-inhibition. Nat. Rev. Immunol. *13*, 227–242. https://doi.org/10.1038/nri3405.

13. Mueller, D.L., Jenkins, M.K., and Schwartz, R.H. (1989). Clonal Expansion Versus Functional Clonal Inactivation: A Costimulatory Signalling Pathway Determines the Outcome of T Cell Antigen Receptor Occupancy. Annu. Rev. Immunol. *7*, 445–480. https://doi.org/10.1146/annurev.iy.07.040189.002305.

14. Curtsinger, J.M., and Mescher, M.F. (2010). Inflammatory Cytokines as a Third Signal for T Cell Activation. Curr. Opin. Immunol. *22*, 333–340. https://doi.org/10.1016/j.coi.2010.02.013.

15. Kaech, S.M., Wherry, E.J., and Ahmed, R. (2002). Effector and memory T-cell differentiation: implications for vaccine development. Nat. Rev. Immunol. *2*, 251–262. https://doi.org/10.1038/nri778.

16. Gebhardt, T., Park, S.L., and Parish, I.A. (2023). Stem-like exhausted and memory $CD8^+$ T cells in cancer. Nat. Rev. Cancer *23*, 780–798. https://doi.org/10.1038/s41568-023-00615-0.

17. Jiang, Y., Li, Y., and Zhu, B. (2015). T-cell exhaustion in the tumor microenvironment. Cell Death Dis. *6*, e1792–e1792. https://doi.org/10.1038/cddis.2015.162.

18. Schnell, A., Bod, L., Madi, A., and Kuchroo, V.K. (2020). The yin and yang of co-inhibitory receptors: toward anti-tumor immunity without autoimmunity. Cell Res. *30*, 285–299. https://doi.org/10.1038/s41422-020-0277-x.

19. The epigenetic landscape of T cell exhaustion - PMC https://pmc.ncbi.nlm.nih.gov/articles/PMC5497589/.

20. Kaech, S.M., and Cui, W. (2012). Transcriptional control of effector and memory CD8$^+$ T cell differentiation. Nat. Rev. Immunol. *12*, 749–761. https://doi.org/10.1038/nri3307.

21. Maru, S., Jin, G., Schell, T.D., and Lukacher, A.E. (2017). TCR stimulation strength is inversely associated with establishment of functional brain-resident memory CD8$^+$ T cells during persistent viral infection. PLOS Pathog. *13*, e1006318. https://doi.org/10.1371/journal.ppat.1006318.

22. Au-Yeung, B.B., Zikherman, J., Mueller, J.L., Ashouri, J.F., Matloubian, M., Cheng, D.A., Chen, Y., Shokat, K.M., and Weiss, A. (2014). A sharp T-cell antigen receptor signaling threshold for T-cell proliferation. Proc. Natl. Acad. Sci. U. S. A. *111*, E3679-3688. https://doi.org/10.1073/pnas.1413726111.

23. King, C.G., Koehli, S., Hausmann, B., Schmaler, M., Zehn, D., and Palmer, E. (2012). T Cell Affinity Regulates Asymmetric Division, Effector Cell Differentiation, and Tissue Pathology. Immunity *37*, 709–720. https://doi.org/10.1016/j.immuni.2012.06.021.

24. Solouki, S., Huang, W., Elmore, J., Limper, C., Huang, F., and August, A. (2020). TCR Signal Strength and Antigen Affinity Regulate CD8$^+$Memory T Cells. J. Immunol. *205*, 1217–1227. https://doi.org/10.4049/jimmunol.1901167.

25. Krummey, S.M., Martinez, R.J., Andargachew, R., Liu, D., Wagener, M., Kohlmeier, J.E., Evavold, B.D., Larsen, C.P., and Ford, M.L. (2016). Low Affinity Memory CD8$^+$ T Cells Mediate Robust Heterologous Immunity. J. Immunol. Baltim. Md 1950 *196*, 2838–2846. https://doi.org/10.4049/jimmunol.1500639.

26. Zehn, D., Lee, S.Y., and Bevan, M.J. (2009). Complete but curtailed T cell response to very low affinity antigen. Nature *458*, 211–214. https://doi.org/10.1038/nature07657.

27. Brownlie, R.J., and Zamoyska, R. (2013). T cell receptor signalling networks: branched, diversified and bounded. Nat. Rev. Immunol. *13*, 257–269. https://doi.org/10.1038/nri3403.

28. Wither, M.J., White, W.L., Pendyala, S., Leanza, P.J., Fowler, D., and Kueh, H.Y. (2023). Antigen perception in T cells by long-term Erk and NFAT signaling dynamics. bioRxiv. https://doi.org/10.1101/2023.06.01.543260.

29. Kalia, V., Sarkar, S., Subramaniam, S., Haining, W.N., Smith, K.A., and Ahmed, R. (2010). Prolonged Interleukin-2Rα Expression on Virus-Specific CD8$^+$ T Cells Favors Terminal-Effector Differentiation In Vivo. Immunity *32*, 91–103. https://doi.org/10.1016/j.immuni.2009.11.010.

30. Harberts, A., Schmidt, C., Schmid, J., Reimers, D., Koch-Nolte, F., Mittrücker, H.-W., and Raczkowski, F. (2021). Interferon regulatory factor 4 controls effector functions of CD8$^+$memory T cells. Proc. Natl. Acad. Sci. *118*, e2014553118. https://doi.org/10.1073/pnas.2014553118.

31. Richard, A.C., Lun, A.T.L., Lau, W.W.Y., Göttgens, B., Marioni, J.C., and Griffiths, G.M. (2018). T cell cytolytic capacity is independent of initial stimulation strength. Nat. Immunol. *19*, 849–858. https://doi.org/10.1038/s41590-018-0160-9.

32. Man, K., Gabriel, S.S., Liao, Y., Gloury, R., Preston, S., Henstridge, D.C., Pellegrini, M.,

Zehn, D., Berberich-Siebelt, F., Febbraio, M.A., et al. (2017). Transcription Factor IRF4 Promotes CD8$^+$ T Cell Exhaustion and Limits the Development of Memory-like T Cells during Chronic Infection. Immunity *47*, 1129-1141.e5. https://doi.org/10.1016/j.immuni.2017.11.021.

33. Yao, S., Buzo, B.F. d., Pham, D., Jiang, L., Taparowsky, E.J., Kaplan, M.H., and Sun, J. (2013). Interferon regulatory factor 4 sustains CD8$^+$ T cell expansion and effector differentiation. Immunity *39*, 10.1016/j.immuni.2013.10.007. https://doi.org/10.1016/j.immuni.2013.10.007.

34. Shin, H., Blackburn, S.D., Intlekofer, A.M., Kao, C., Angelosanto, J.M., Reiner, S.L., and Wherry, E.J. (2009). A role for the transcriptional repressor Blimp-1 in CD8$^+$ T cell exhaustion during chronic viral infection. Immunity *31*, 309–320. https://doi.org/10.1016/j.immuni.2009.06.019.

35. McLane, L.M., Ngiow, S.F., Chen, Z., Attanasio, J., Manne, S., Ruthel, G., Wu, J.E., Staupe, R.P., Xu, W., Amaravadi, R.K., et al. (2021). Role of nuclear localization in the regulation and function of T-bet and Eomes in exhausted CD8$^+$ T cells. Cell Rep. *35*, 109120. https://doi.org/10.1016/j.celrep.2021.109120.

36. Scott, A.C., Dündar, F., Zumbo, P., Chandran, S.S., Klebanoff, C.A., Shakiba, M., Trivedi, P., Menocal, L., Appleby, H., Camara, S., et al. (2019). TOX is a critical regulator of tumour-specific T cell differentiation. Nature *571*, 270–274. https://doi.org/10.1038/s41586-019-1324-y.

37. Yao, C., Sun, H.-W., Lacey, N.E., Ji, Y., Moseman, E.A., Shih, H.-Y., Heuston, E.F., Kirby, M., Anderson, S., Cheng, J., et al. (2019). Single-cell RNA-seq reveals TOX as a key regulator of CD8$^+$ T cell persistence in chronic infection. Nat. Immunol. *20*, 890–901. https://doi.org/10.1038/s41590-019-0403-4.

38. Abadie, K., Clark, E.C., Valanparambil, R.M., Ukogu, O., Yang, W., Daza, R.M., Ng, K.K.H., Fathima, J., Wang, A.L., Lee, J., et al. (2024). Reversible, tunable epigenetic silencing of TCF1 generates flexibility in the T cell memory decision. Immunity *57*, 271-286.e13. https://doi.org/10.1016/j.immuni.2023.12.006.

39. Zhou, X., Yu, S., Zhao, D.-M., Harty, J.T., Badovinac, V.P., and Xue, H.-H. (2010). Differentiation and persistence of memory CD8$^+$ T cells depend on T cell factor 1. Immunity *33*, 229–240. https://doi.org/10.1016/j.immuni.2010.08.002.

40. Beltra, J.-C., Manne, S., Abdel-Hakeem, M.S., Kurachi, M., Giles, J.R., Chen, Z., Casella, V., Ngiow, S.F., Khan, O., Huang, Y.J., et al. (2020). Developmental Relationships of Four Exhausted CD8$^+$ T Cell Subsets Reveals Underlying Transcriptional and Epigenetic Landscape Control Mechanisms. Immunity *52*, 825-841.e8. https://doi.org/10.1016/j.immuni.2020.04.014.

41. Abdel-Hakeem, M.S., Manne, S., Beltra, J.-C., Stelekati, E., Chen, Z., Nzingha, K., Ali, M.-A., Johnson, J.L., Giles, J.R., Mathew, D., et al. (2021). Epigenetic scarring of exhausted T cells hinders memory differentiation upon eliminating chronic antigenic stimulation. Nat. Immunol. *22*, 1008–1019. https://doi.org/10.1038/s41590-021-00975-5.

42. Yates, K.B., Tonnerre, P., Martin, G.E., Gerdemann, U., Al Abosy, R., Comstock, D.E., Weiss, S.A., Wolski, D., Tully, D.C., Chung, R.T., et al. (2021). Epigenetic scars of CD8$^+$ T

cell exhaustion persist after cure of chronic infection in humans. Nat. Immunol. *22*, 1020–1029. https://doi.org/10.1038/s41590-021-00979-1.

43. DNA binding by polycomb-group proteins: searching for the link to CpG islands - PMC https://pmc.ncbi.nlm.nih.gov/articles/PMC9122586/.

44. Angrand, P.-O. (2022). Structure and Function of the Polycomb Repressive Complexes PRC1 and PRC2. Int. J. Mol. Sci. *23*, 5971. https://doi.org/10.3390/ijms23115971.

45. Geng, Z., and Gao, Z. (2020). Mammalian PRC1 Complexes: Compositional Complexity and Diverse Molecular Mechanisms. Int. J. Mol. Sci. *21*, 8594. https://doi.org/10.3390/ijms21228594.

46. Liu, Y., Hu, G., Yang, S., Yao, M., Liu, Z., Yan, C., Wen, Y., Ping, W., Wang, J., Song, Y., et al. (2023). Functional dissection of PRC1 subunits RYBP and YAF2 during neural differentiation of embryonic stem cells. Nat. Commun. *14*, 7164. https://doi.org/10.1038/s41467-023-42507-9.

47. Kim, J., and Kingston, R.E. (2020). The CBX family of proteins in transcriptional repression and memory. J. Biosci. *45*, 16.

48. Shi, Y., Wang, X., Zhuang, Y., Jiang, Y., Melcher, K., and Xu, H.E. (2017). Structure of the PRC2 complex and application to drug discovery. Acta Pharmacol. Sin. *38*, 963–976. https://doi.org/10.1038/aps.2017.7.

49. Zhou, W., Zhu, P., Wang, J., Pascual, G., Ohgi, K.A., Lozach, J., Glass, C.K., and Rosenfeld, M.G. (2008). Histone H2A Monoubiquitination Represses Transcription by Inhibiting RNA Polymerase II Transcriptional Elongation. Mol. Cell *29*, 69–80. https://doi.org/10.1016/j.molcel.2007.11.002.

50. Epigenetic regulation of T cells by Polycomb group proteins | Journal of Leukocyte Biology | Oxford Academic https://academic.oup.com/jleukbio/article/111/6/1253/6885187?login=false.

51. Di Croce, L., and Helin, K. (2013). Transcriptional regulation by Polycomb group proteins. Nat. Struct. Mol. Biol. *20*, 1147–1155. https://doi.org/10.1038/nsmb.2669.

52. Gray, S.M., Amezquita, R.A., Guan, T., Kleinstein, S.H., and Kaech, S.M. (2017). Polycomb repressive complex 2-mediated chromatin repression guides effector $CD8^+$ T cell terminal differentiation and loss of multipotency. Immunity *46*, 596–608. https://doi.org/10.1016/j.immuni.2017.03.012.

53. Chen, G., Subedi, K., Chakraborty, S., Sharov, A., Lu, J., Kim, J., Mi, X., Wersto, R., Sung, M.-H., and Weng, N. (2018). Ezh2 Regulates Activation-Induced $CD8^+$ T Cell Cycle Progression via Repressing Cdkn2a and Cdkn1c Expression. Front. Immunol. *9*. https://doi.org/10.3389/fimmu.2018.00549.

54. Gerhardt, L., Hong, M.M.Y., Yousefi, Y., Figueredo, R., and Maleki Vareki, S. (2023). IL-12 and IL-27 Promote CD39 Expression on $CD8^+$ T Cells and Differentially Regulate the CD39+$CD8^+$ T Cell Phenotype. J. Immunol. Author Choice *210*, 1598–1606. https://doi.org/10.4049/jimmunol.2200897.

55. Danilo, M., Chennupati, V., Silva, J.G., Siegert, S., and Held, W. (2018). Suppression of Tcf1 by Inflammatory Cytokines Facilitates Effector CD8$^+$ T Cell Differentiation. Cell Rep. *22*, 2107–2117. https://doi.org/10.1016/j.celrep.2018.01.072.

56. Scott-Browne, J.P., López-Moyado, I.F., Trifari, S., Wong, V., Chavez, L., Rao, A., and Pereira, R.M. (2016). Dynamic changes in chromatin accessibility in CD8$^+$ T cells responding to viral infection. Immunity *45*, 1327–1340. https://doi.org/10.1016/j.immuni.2016.10.028.

57. Ford, B.R., Vignali, P.D.A., Rittenhouse, N.L., Scharping, N.E., Peralta, R., Lontos, K., Frisch, A.T., Delgoffe, G.M., and Poholek, A.C. (2022). Tumor microenvironmental signals reshape chromatin landscapes to limit the functional potential of exhausted T cells. Sci. Immunol. *7*, eabj9123. https://doi.org/10.1126/sciimmunol.abj9123.

58. Hosogane, M., Funayama, R., Shirota, M., and Nakayama, K. (2016). Lack of Transcription Triggers H3K27me3 Accumulation in the Gene Body. Cell Rep. *16*, 696–706. https://doi.org/10.1016/j.celrep.2016.06.034.

59. Krug, B., Hu, B., Chen, H., Ptack, A., Chen, X., Gretarsson, K.H., Deshmukh, S., Kabir, N., Andrade, A.F., Jabbour, E., et al. (2023). H3K27me3 spreading organizes canonical PRC1 chromatin architecture to regulate developmental programs. bioRxiv, 2023.11.28.567931. https://doi.org/10.1101/2023.11.28.567931.

60. Nolz, J.C., and Richer, M.J. (2020). Control of memory CD8$^+$ T cell longevity and effector functions by IL-15. Mol. Immunol. *117*, 180–188. https://doi.org/10.1016/j.molimm.2019.11.011.

61. Jadhav, U., Manieri, E., Nalapareddy, K., Madha, S., Chakrabarti, S., Wucherpfennig, K., Barefoot, M., and Shivdasani, R.A. (2020). Replicational Dilution of H3K27me3 in Mammalian Cells and the Role of Poised Promoters. Mol. Cell *78*, 141-151.e5. https://doi.org/10.1016/j.molcel.2020.01.017.

62. Nekrasov, M., Klymenko, T., Fraterman, S., Papp, B., Oktaba, K., Köcher, T., Cohen, A., Stunnenberg, H.G., Wilm, M., and Müller, J. (2007). Pcl-PRC2 is needed to generate high levels of H3-K27 trimethylation at Polycomb target genes. EMBO J. *26*, 4078–4088. https://doi.org/10.1038/sj.emboj.7601837.

63. Loubière, V., Delest, A., Thomas, A., Bonev, B., Schuettengruber, B., Sati, S., Martinez, A.-M., and Cavalli, G. (2016). Coordinate redeployment of PRC1 proteins suppresses tumor formation during Drosophila development. Nat. Genet. *48*, 1436–1442. https://doi.org/10.1038/ng.3671.

64. Guerard-Millet, F., Gentile, C., Paul, R., Mayran, A., and Kmita, M. (2021). Polycomb Repressive Complexes occupancy reveals PRC2-independent PRC1 critical role in the control of limb development. https://doi.org/10.1101/2021.10.28.466236.

65. McCole, R., Nolan, J., Reck, D.M., Monger, C., Rustichelli, S., Conway, E., Brien, G.L., Wang, C., Deevy, O., Neikes, H.K., et al. (2025). A conserved switch to less catalytically active Polycomb repressive complexes in non-dividing cells. Cell Rep. *44*, 115192. https://doi.org/10.1016/j.celrep.2024.115192.

66. Dynamic PRC1–CBX8 stabilizes a porous structure of chromatin condensates | Nature

Structural & Molecular Biology https://www.nature.com/articles/s41594-024-01457-6.

67. Healy, E., and Bracken, A.P. (2020). If You Like It Then You Shoulda Put Two “RINGs” on It: Delineating the Roles of vPRC1 and cPRC1. Mol. Cell *77*, 685–687. https://doi.org/10.1016/j.molcel.2020.02.002.

68. Zepeda-Martinez, J.A., Pribitzer, C., Wang, J., Bsteh, D., Golumbeanu, S., Zhao, Q., Burkard, T.R., Reichholf, B., Rhie, S.K., Jude, J., et al. (2020). Parallel PRC2/cPRC1 and vPRC1 pathways silence lineage-specific genes and maintain self-renewal in mouse embryonic stem cells. Sci. Adv. *6*, eaax5692. https://doi.org/10.1126/sciadv.aax5692.

69. Kansy, B.A., Concha-Benavente, F., Srivastava, R.M., Jie, H.-B., Shayan, G., Lei, Y., Moskovitz, J., Moy, J., Li, J., Brandau, S., et al. (2017). PD-1 status in $CD8^+$ T cells associates with survival and anti-PD-1 therapeutic outcomes in head and neck cancer. Cancer Res. *77*, 6353–6364. https://doi.org/10.1158/0008-5472.CAN-16-3167.

70. Lugli, E., Galletti, G., Boi, S.K., and Youngblood, B.A. (2020). Stem, effector and hybrid states of memory $CD8^+$ T cells. Trends Immunol. *41*, 17–28. https://doi.org/10.1016/j.it.2019.11.004.

71. Yang, S., Liu, F., Wang, Q.J., Rosenberg, S.A., and Morgan, R.A. (2011). The Shedding of CD62L (L-Selectin) Regulates the Acquisition of Lytic Activity in Human Tumor Reactive T Lymphocytes. PLoS ONE *6*, e22560. https://doi.org/10.1371/journal.pone.0022560.

72. Blackledge, N.P., and Klose, R.J. (2021). The molecular principles of gene regulation by Polycomb repressive complexes. Nat. Rev. Mol. Cell Biol. *22*, 815–833. https://doi.org/10.1038/s41580-021-00398-y.

73. The transcription factor TCF-1 enforces commitment to the innate lymphoid cell lineage - PMC https://pmc.ncbi.nlm.nih.gov/articles/PMC6707869/.

74. Zhu, L.J., Gazin, C., Lawson, N.D., Pagès, H., Lin, S.M., Lapointe, D.S., and Green, M.R. (2010). ChIPpeakAnno: a Bioconductor package to annotate ChIP-seq and ChIP-chip data. BMC Bioinformatics *11*, 237. https://doi.org/10.1186/1471-2105-11-237.